The Astrophysical Journal, 717:617–639, 2010 July 10 doi:10.1088/0004-637X/717/2/617

THE VELOCITY DISTRIBUTION OF NEARBY STARS FROM *HIPPARCOS* DATA. II. THE NATURE OF THE LOW-VELOCITY MOVING GROUPS

Jo Bovy[1,3] and David W. Hogg[1,2]
[1] Center for Cosmology and Particle Physics, Department of Physics, New York University, 4 Washington Place, New York, NY 10003, USA; jo.bovy@nyu.edu
[2] Max-Planck-Institut für Astronomie, Königstuhl 17, D-69117 Heidelberg, Germany
Received 2009 December 16; accepted 2010 May 7; published 2010 June 16

ABSTRACT

The velocity distribution of nearby stars ($\lesssim$100 pc) contains many overdensities or "moving groups," clumps of comoving stars, that are inconsistent with the standard assumption of an axisymmetric, time-independent, and steady-state Galaxy. We study the age and metallicity properties of the low-velocity moving groups based on the reconstruction of the local velocity distribution in Paper I of this series. We perform stringent, conservative hypothesis testing to establish for each of these moving groups whether it could conceivably consist of a coeval population of stars. We conclude that they do not: the moving groups are neither trivially associated with their eponymous open clusters nor with any other inhomogeneous star formation event. Concerning a possible dynamical origin of the moving groups, we test whether any of the moving groups has a higher or lower metallicity than the background population of thin disk stars, as would generically be the case if the moving groups are associated with resonances of the bar or spiral structure. We find clear evidence that the Hyades moving group has higher than average metallicity and weak evidence that the Sirius moving group has lower than average metallicity, which could indicate that these two groups are related to the inner Lindblad resonance of the spiral structure. Further, we find weak evidence that the Hercules moving group has higher than average metallicity, as would be the case if it is associated with the bar's outer Lindblad resonance. The Pleiades moving group shows no clear metallicity anomaly, arguing against a common dynamical origin for the Hyades and Pleiades groups. Overall, however, the moving groups are barely distinguishable from the background population of stars, raising the likelihood that the moving groups are associated with transient perturbations.

Key words: Galaxy: fundamental parameters – Galaxy: kinematics and dynamics – Galaxy: structure – methods: statistical – solar neighborhood – stars: kinematics and dynamics

1. INTRODUCTION

Moving groups—clumps of stars in the solar neighborhood sharing the same space velocity—have been known for over a century (Mädler 1846; Proctor 1869) and their interpretation has touched on some of the most basic facts about our Galaxy and the universe. From the location of the center of the Milky Way (Mädler 1847) to the age and dynamical state of the universe (Jeans 1915, 1935; Bok 1946), presently, the moving groups are used to constrain the dynamical properties of the Galactic disk (e.g., Dehnen 2000; Quillen & Minchev 2005). However, in order to quantitatively constrain the fundamental properties of the Galaxy using the presence of structure in the local velocity distribution, the nature of the moving groups needs to be clarified. At present, the evidence that the moving groups are not unmixed structures in phase space consisting of the ghosts of past star formation events, but are instead dynamical effects arising from non-axisymmetric components of the Galaxy's mass distribution, is by and large circumstantial. Currently, any constraint on Galaxy dynamics arising from the moving groups' existence or properties is subject to the large uncertainty as to what the actual origin of the moving groups is.

The structure of the local velocity distribution has received much attention during the last century. While the simplest assumption is that the distribution of velocities is a simple Gaussian distribution (Schwarzschild 1907), this assumption was untenable in light of observations that showed the presence of multiple "streams" in the velocity distribution (Kapteyn 1905; Eddington 1910). That these streams are very prominent and make up a large part of the full distribution is clear from the fact that their existence was so readily established. Until the *Hipparcos* mission, the actual contribution of the substructure to the velocity distribution was only poorly characterized, but the rich *Hipparcos* data set conclusively showed that a large fraction of the local velocity distribution is in the form of clumps (Dehnen 1998; Skuljan et al. 1999); a quantitative analysis shows that about 40% of the stars in the solar neighborhood ($\lesssim$100 pc) is part of a small number of moving groups (Bovy et al. 2009a). The velocity distribution with the moving groups indicated is shown in Figure 1.

The nature and origin of the moving groups has remained elusive all this time, although considerable effort has been made both observationally and theoretically to explain and interpret the existence of the moving groups. For much of the last century the consensus view was that the moving groups are the remnants of past star formation events, coeval populations of stars that were once closely associated in position as well as velocity but that have now dispersed and spread out over vast regions of space into the loose associations of stars that still retain a common motion. This view of a dynamically unrelaxed Galaxy was first expressed by Jeans (1915) and its most vociferous proponent during the second half of the century was Eggen (e.g., Eggen 1996). The Hyades and Ursa Major moving groups seemed to fit into this framework as disrupting clusters in a differentially rotating disk (Bok 1934, 1936, 1946). The inspection of the properties of likely Hyades members showed that these followed a similar color–luminosity relation as the Hyades and Praesepe open clusters (Eggen 1958), which seemed to vindicate the view of moving groups as disrupting clusters. This explanation of the

[3] Author to whom any correspondence should be addressed.

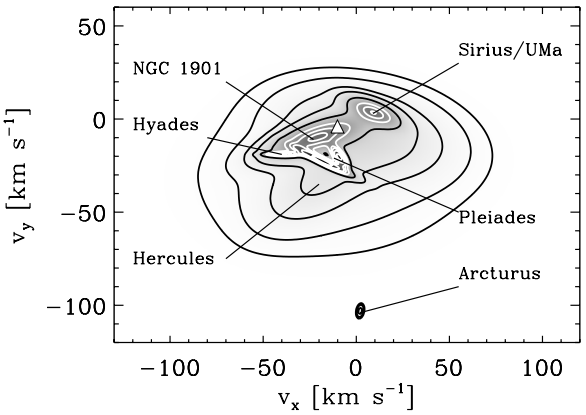

Figure 1. Velocity distribution in the solar neighborhood (from Bovy et al. 2009a) in the Galactic plane with the moving groups studied in this work indicated. The density grayscale is linear and contours contain, from the inside outward, 2%, 6%, 12%, 21%, 33%, 50%, 68%, 80%, 90%, and 95% of the distribution. The first five of these contours are white and somewhat blended together; 50% of the distribution is contained within the innermost dark contour. The origin in each of these plots is at the solar velocity; the velocity of the local standard of rest (Hogg et al. 2005) is indicated by a triangle.

moving groups' origins was contested, however (e.g., Breger 1968; Wielen 1971; Williams 1971; Soderblom & Clemens 1987; Boesgaard & Budge 1988), and started to fall out of favor by the end of the century as observational evidence started to appear that moving group members were a much more varied population of stars than the open clusters with which they were believed to be associated: Eggen (1993) found that the Hyades moving group has a different luminosity function than the Hyades open cluster; Dehnen (1998) found that moving groups are present in various color subsamples of *Hipparcos* stars and that therefore, using color as a proxy for mean age, moving groups contain stars of a wide range of ages. Nevertheless, the evaporating cluster narrative still holds sway for (parts of) some moving groups (Asiain et al. 1999), in particular for the small HR 1614 moving group (Feltzing & Holmberg 2000; De Silva et al. 2007), which we do not study here because it does not stand out as a kinematic overdensity in the overall velocity distribution. In Sections 3 and 6, we ask whether the moving groups constitute a single-burst stellar population.

In the last decade, there have been various indications that the moving groups might have a dynamical origin. The Hercules moving group in particular, an overdensity offset from the bulk of the velocity distribution opposite the direction of Galactic rotation, displays a wide range of metallicities (Raboud et al. 1998; Bensby et al. 2007) and consists mainly of old stars (Caloi et al. 1999; see also the earlier work by Blaauw 1970). The Hyades moving groups also seemed to contain both old and young stars (Chereul & Grenon 2001), and soon all low-velocity moving groups—excluding higher velocity features such as the Arcturus moving group—were suspected of having a dynamical origin (Famaey et al. 2005, 2007, 2008).

Theoretical considerations and simulations of orbits in non-axisymmetric potentials such as that corresponding to the Galactic bar or spiral structure also contributed to the belief that moving groups might not be evaporating clusters of stars. The observed pattern of moving groups can be thought of quite naturally as arising from the bifurcation of orbits near resonances associated with the bar (Kalnajs 1991; Dehnen 2000; Fux 2001) or steady-state spiral structure (Quillen & Minchev 2005). Other simulations have shown that moving-group-like structures also develop when considering transient spiral structure (De Simone et al. 2004), recent bar growth (Minchev et al. 2009), or the combined effect of spiral structure and spiral arms (Quillen 2003; Chakrabarty 2007; Antoja et al. 2009). These dynamical scenarios for the origin of the moving groups are discussed in more detail in Section 7, in which we test several of these dynamical scenarios.

Most of the non-axisymmetric perturbations that have been proposed to create the moving groups are associated with stable, long-lived perturbations, e.g., a long-lived density wave (Lin & Shu 1964). However, several pieces of evidence indicate that spiral structure might be only short-lived and/or transient: spiral structure gradually heats the disk (Carlberg & Sellwood 1985) such that it eventually becomes stable against non-axisymmetric perturbations in the absence of a cooling mechanism (Sellwood & Carlberg 1984); spiral density waves tend to dissipate within a few galactic revolutions if fresh waves are not continuously created (Toomre 1969); spiral structure is more common in high density environments than in the field (Elmegreen & Elmegreen 1982, 1983) where interactions between galaxies that could induce transient spiral structure are more common; and nearby galaxies show strong variations of the pattern speed with galactocentric radius, which strongly constrains the lifetime of grand-design spiral structure (Merrifield et al. 2006; Meidt et al. 2009). The velocity distribution inferred from the *Hipparcos* data itself, with its large amount of substructure, shows that spiral structure does not operate on a smooth phase-space density and that spiral instabilities that grow because of features in the phase-space distribution (e.g., Sellwood & Lin 1989; Sellwood & Kahn 1991) should therefore be expected to be present.

One such instability driven by features in the angular-momentum distribution such as grooves or ridges is the scenario proposed by Sellwood & Kahn (1991; see also Lovelace & Hohlfeld 1978). In this model for the growth of spiral modes, an initial narrow groove in the angular-momentum density grows into a well-defined large-scale spiral pattern that dies off again after a few galactic rotations (at corotation, which lies near the groove center). Since stars are scattered at the inner Lindblad resonance (ILR) of the spiral pattern, an underdensity of stars in energy–angular-momentum space forms at the Lindblad resonance, which could spur a new cycle of growth of a spiral instability, albeit with a corotation radius near the ILR of the previous pattern. Since the corotation radii of subsequent spiral patterns move steadily inward, this recurrent cycle stops at a certain point. In Section 8, we ask whether any of the moving groups is a manifestation of this scenario.

Although the *Hipparcos* data allowed the velocity distribution in the solar neighborhood to be studied in detail for the first time using complete samples of stars, and theoretical work on the origin of the moving groups has blossomed in recent years, little progress has been made observationally to elucidate the nature of the moving groups. In this paper, we use large samples of *Hipparcos* stars—an order of magnitude improvement over previous studies—to investigate the origin of the kinematical substructures seen in Figure 1. We use the reconstruction of the local velocity distribution from Bovy et al. (2009a) to assign moving-group membership probabilities to the stars. We propagate the membership uncertainty through all of the analyses of the properties of the moving-group member stars. This avoids all of the biases that result from making hard cuts on membership in investigations of this kind and allows us to perform comprehensive tests to establish the origin of each individual moving group.

Before we continue, it is worth pointing out that OB associations—spatially localized associations of young stars (e.g., de Zeeuw et al. 1999)—are also sometimes referred to as moving groups. The following does *not* concern these OB associations.

The main parts of this paper are the following. In Section 3, we show that the moving groups are not associated with their eponymous open clusters; in Section 6, we extend this result to show that the moving groups are not associated with any single episode of star formation; in Section 7, we test whether the moving groups arise because of steady-state dynamical perturbations to the axisymmetric disk potential; and in Section 8, we look at whether the moving groups are associated with the recurrent spiral structure scenario of Sellwood & Kahn (1991).

2. DATA

We use the standard Galactic velocity coordinate system, with the directions x, y, and z (and associated unit vectors $\hat{\mathbf{x}}$, $\hat{\mathbf{y}}$, and $\hat{\mathbf{z}}$) pointing toward the Galactic center, in the direction of the circular orbital motion, and toward the north Galactic pole, respectively. Vectors are everywhere taken to be column vectors. The components of the velocity vector, $\hat{\mathbf{x}}^\top\mathbf{v}$, $\hat{\mathbf{y}}^\top\mathbf{v}$, and $\hat{\mathbf{z}}^\top\mathbf{v}$, are conventionally referred to as U, V, and W, respectively, but we will refer to them as v_x, v_y, and v_z.

2.1. Sample Selection

We follow the procedure of Dehnen & Binney (1998) and Aumer & Binney (2009) in selecting a magnitude-limited, kinematically unbiased sample of single main-sequence stars with accurate astrometry from the *Hipparcos* catalog. We start by determining the magnitude to which the *Hipparcos* catalog is complete in 16 × 16 × 10 equal width bins in $\sin b$, l, and color $B_\mathrm{T} - V_\mathrm{T}$, the latter measured in the *Tycho* passbands in the interval $(-0.3,1.5)$, by finding the V_T magnitude of the second brightest star that is included in the *Tycho* catalog (Høg et al. 2000a, 2000b), but absent in the *Hipparcos* catalog. We then select in each bin all stars from the original *Hipparcos* catalog (ESA 1997) brighter in V_T than the limiting magnitude in that bin. From this sample of stars we select single stars by using the "Solution type" $\mathrm{isol}_n < 10$ in the new reduction of the *Hipparcos* data (van Leeuwen 2007), and stars with accurate astrometry by selecting stars with relative parallax uncertainties smaller than 10% (using the formal error on the parallax in the new *Hipparcos* catalog). Main-sequence stars are selected by using the color–magnitude cuts from Aumer & Binney (2009):

$$\begin{aligned}
&M_\mathrm{Hip} < 7.50 \times (B-V) - 3.75\,, && B-V \leqslant 0.5\\
&M_\mathrm{Hip} < 15.33 \times (B-V) - 7.665\,, && 0.5 \leqslant B-V \leqslant 0.8\\
&M_\mathrm{Hip} < 4.43 \times (B-V) + 1.055\,, && 0.8 \leqslant B-V\\
&M_\mathrm{Hip} > 4.62 \times (B-V) + 2.383\,, && B-V \leqslant 0.35\\
&M_\mathrm{Hip} > 8.33 \times (B-V) + 1.0845\,, && 0.35 \leqslant B-V \leqslant 0.65\\
&M_\mathrm{Hip} > 3.33 \times (B-V) + 4.3375\,, && 0.65 \leqslant B-V \leqslant 1.25\\
&M_\mathrm{Hip} > 6.50 \times (B-V) + 0.375\,, && 1.25 \leqslant B-V,
\end{aligned} \tag{1}$$

where M_Hip is the absolute magnitude in *Hipparcos*' own passband.

This procedure selects 19,631 stars from the *Hipparcos* catalog, 15,023 of which are main-sequence stars. The color–magnitude diagram of the full sample of 19,631 stars is shown in Figure 2; the cuts defining the main-sequence are also shown in this figure.

We refer the reader to Bovy et al. (2009a, hereafter BHR) for a detailed explanation of how three-dimensional velocities are projected onto the two-dimensional tangential plane observed by *Hipparcos*—since the *Hipparcos* mission did not measure radial velocities, this third velocity component is missing for all of the stars in the sample—and how the uncertainties given in the *Hipparcos* catalog are propagated to the uncertainties in the tangential velocity components. In what follows, $\mathbf{w}_i$ will represent the observed tangential velocity of star i, $\mathbf{v}_i$ its (unobserved) three-dimensional velocity, $\mathbf{R}_i$ the projection matrix onto the tangential plane for star i—i.e., $\mathbf{R}_i\mathbf{v}_i = \mathbf{w}_i$—and $\mathbf{S}_i$ the two-dimensional observational-uncertainty variance matrix in the tangential-velocity plane.

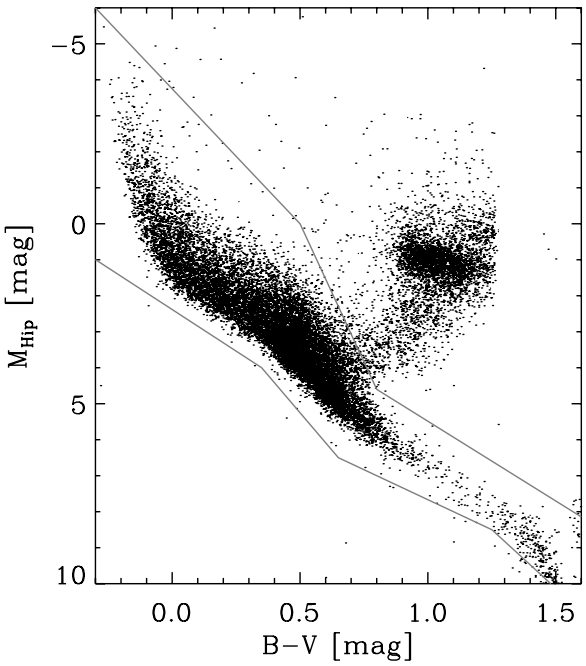

Figure 2. Color–magnitude diagram of the full *Hipparcos* sample of 19,631 stars, selected to be kinematically unbiased and consists of single stars with relative parallax uncertainties $\lesssim 10\%$. The 15,023 main-sequence stars that we use in the hypothesis tests in Sections 3, 5, and 6 lie between the gray lines. M_Hip is the absolute magnitude in *Hipparcos*' own passband.

2.2. Probabilistic Moving-group Membership Determination

BHR reconstructed the velocity distribution of nearby stars by deconvolving the observed tangential velocity distribution of a kinematically unbiased sample of 11,865 *Hipparcos* stars. The deconvolution algorithm (Bovy et al. 2009b) represents the underlying velocity distribution as a sum, or mixture, of Gaussian components and can properly handle arbitrary uncertainties, including missing data, provided that there are no significant star-to-star correlations. These are believed to be insignificant in the most recent release of the *Hipparcos* data (van Leeuwen 2007). Model selection, most notably the selection of the "right" number of components in the mixture, was based on predicting the radial velocities in the *Geneva–Copenhagen Survey* (GCS; Nordström et al. 2004). BHR found that the underlying three-dimensional velocity distribution was best represented by a 10-component mixture of Gaussians and found the 99 best-fit parameters of this decomposition.

Although in Gaussian-mixture deconvolution the individual components do not necessarily have any meaningful interpretation—the Gaussians are simply the basis functions of an expansion—many of the Gaussian components in the best-fit mixture could be identified unambiguously with peaks in the velocity

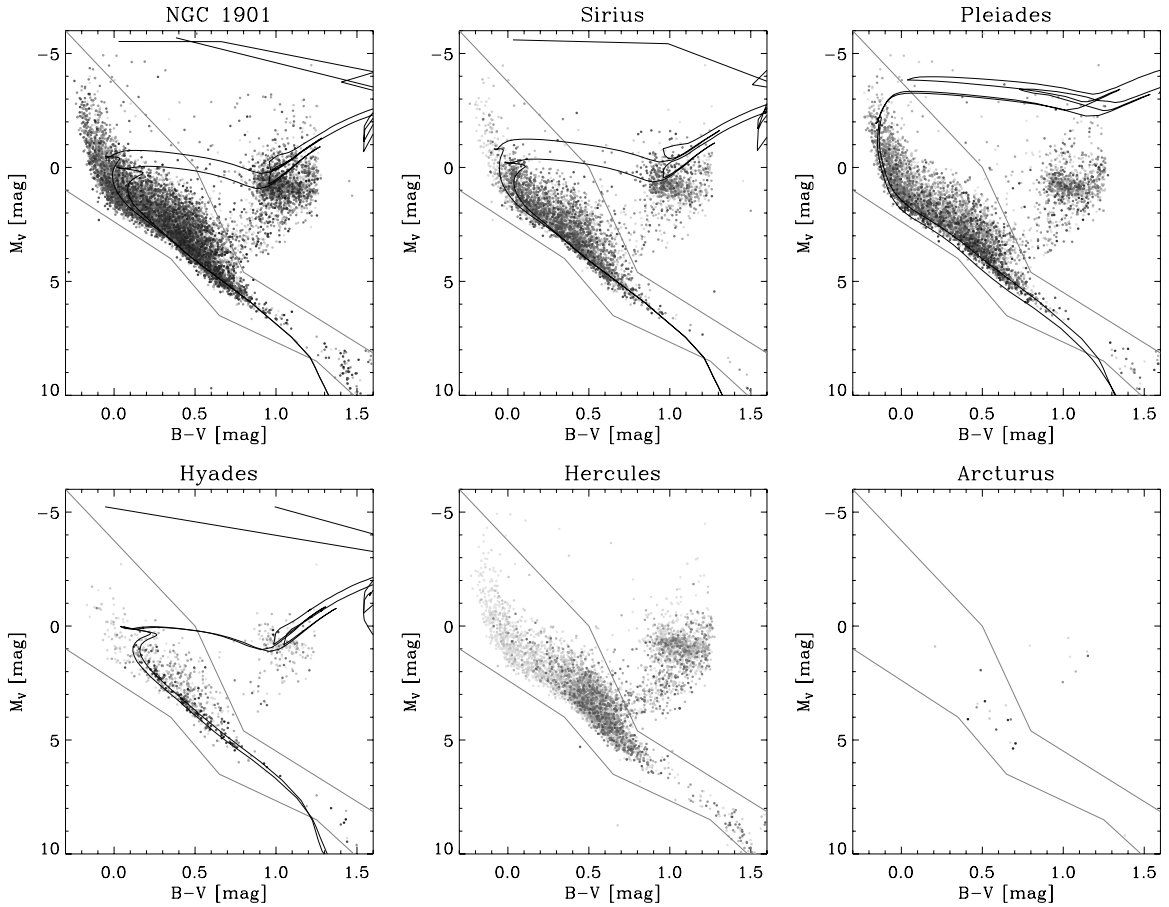

Figure 3. Color–magnitude diagrams of the six moving groups detected in BHR. The points are grayscale-coded with the probability of each star to be part of the moving group (see the text); only stars that have a probability larger than 0.1 of being part of the moving group are plotted. For those moving groups potentially associated with an open cluster, theoretical isochrones (Marigo et al. 2008; Bertelli et al. 1994) for the open cluster are overlaid: the 400 Myr, $Z = 0.016$ (Carraro et al. 2007) and the 600 Myr, $Z = 0.016$ (Pavani et al. 2001) isochrone for the NGC 1901 cluster; the 300 Myr, $Z = 0.016$ (Soderblom & Mayor 1993) and the 500 Myr, $Z = 0.016$ (King et al. 2003) isochrone for the Ursa Major (Sirius) cluster; the 100 Myr, $Z = 0.018$ (Boesgaard & Friel 1990; Gratton 2000) and the 100 Myr, $Z = 0.008$ (Percival et al. 2005) isochrone for the Pleiades cluster; the 625 Myr, $Z = 0.026$ isochrone (Perryman et al. 1998) and the 625 Myr, $Z = 0.019$ isochrone for the Hyades cluster. The main-sequence cuts from Figure 2 are indicated in gray.

distribution, most of which correspond to known moving groups. For the purposes of this paper we will use the representation of the velocity distribution as a mixture of 10 Gaussian components with the parameters given in Table 1 of BHR; we will come back to this choice in the discussion in Section 9. We will identify the main moving groups in the velocity distribution with the components in Table 1 of BHR as follows: component 2 corresponds to the NGC 1901 moving group; component 4 to the Hercules moving group; component 5 to the Sirius moving group; components 6 and 7 to the Pleiades moving group; component 8 to the Hyades moving group; and component 10 to the Arcturus moving group.

We can now probabilistically assign stars to Gaussian components or moving groups. For each star i we calculate the probability that it is associated with component j of the Gaussian mixture model for the local velocity distribution

$$p_{ij} = \frac{\alpha_j \, \mathcal{N}\left(\mathbf{w}_i | \mathbf{R}_i \mathbf{m}_j, \mathbf{R}_i \mathbf{V}_j \mathbf{R}_i^\top + \mathbf{S}_i\right)}{\sum_k \alpha_k \, \mathcal{N}\left(\mathbf{w}_i | \mathbf{R}_i \mathbf{m}_k, \mathbf{R}_i \mathbf{V}_k \mathbf{R}_i^\top + \mathbf{S}_i\right)}, \qquad (2)$$

where $\alpha_j, \mathbf{m}_j, \mathbf{V}_j$ are the amplitude, mean, and variance of the jth Gaussian component, which are given in Table 1 of BHR; see Bovy et al. (2009b) for a derivation of this formula. For the Pleiades moving group for each star i we add up the probabilities of it being associated with component 6 or 7, i.e., $p_{i,\mathrm{Pleiades}} = p_{i6} + p_{i7}$, since two of the components of the mixture are associated with the Pleiades moving group (see BHR for an extended discussion of this).

3. A FIRST LOOK: ARE THE LOW-VELOCITY MOVING GROUPS ASSOCIATED WITH THEIR EPONYMOUS OPEN CLUSTERS?

To get a first idea about the properties of the moving groups we can look at "probabilistic" color–magnitude diagrams of the groups, which will form the basis for everything we do in the remainder of this paper. Using the probabilities p_{ij} for each star i to be part of moving group j, we can create color–magnitude diagrams for the different moving groups that are weighted by the probabilities of each star to be part of that particular moving group. Such color–magnitude diagrams are shown in Figure 3 for the six moving groups unambiguously detected by BHR. In these color–magnitude diagrams, each star is plotted as a dot with the grayscale of that dot proportional to the probability of the star to be part of the moving group. For clarity only those stars with $p_{ij} > 0.1$ are plotted. It is clear from this figure that very few stars can be associated with the Arcturus moving group. For this reason, we will not discuss the Arcturus moving group in this paper; instead, we will focus on the remaining, low-velocity, moving groups.

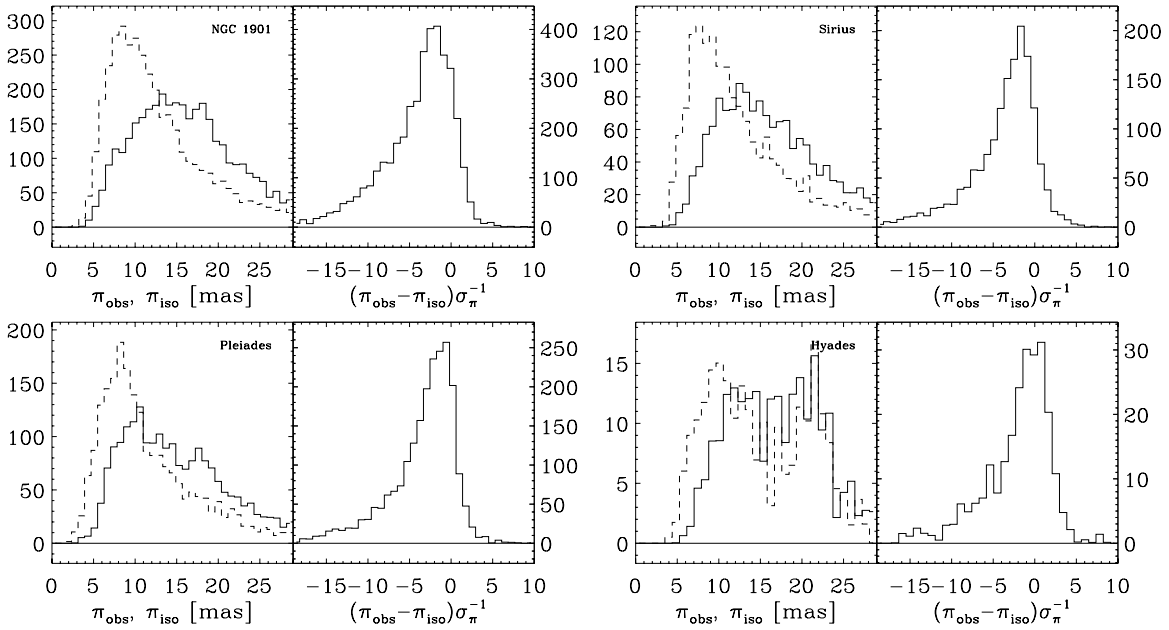

Figure 4. Observed parallaxes vs. model parallaxes assuming a single-burst stellar population identical to that of the associated cluster of the moving groups: comparison of the distribution of observed parallaxes (dashed lines) with that of the model parallaxes (solid lines) in the left figure of each panel; histogram of the normalized difference between model and observed parallax in the right figure. Each star is weighted by its probability of being part of the moving group in question. The isochrone used in this figure corresponds to the first age and metallicity pair mentioned in the caption of Figure 3 for each open cluster.

The color–magnitude relation of the low-velocity moving groups in Figure 3 is very broad for each of the moving groups. Care must be taken, however, in interpreting this fact, since the effect of parallax uncertainties is not shown in this figure and the observed scatter in the color–magnitude relation might well have some contribution from this uncertainty propagated. We will come back to this question below. More disturbing, therefore, is the systematic offset between the color–magnitude relation of the moving group and the isochrone of the open cluster associated with the moving group. No open cluster is associated with the Hercules moving group, and we will therefore ignore it for the remainder of this section.

Two isochrones in the BV photometric system (Marigo et al. 2008; Bertelli et al. 1994; Maíz Apellániz 2006)[4] are plotted for each of the moving groups corresponding to the proposed ages and metallicities for the associated open clusters found in the literature; see the caption of Figure 3 for the details on each open cluster. It is clear from this figure that the isochrones of the open clusters do not represent the color–magnitude relation of their associated moving groups well, although a caveat remains about the effect of parallax uncertainties and the effect of low-probability moving group members, which is hard to gauge from this figure. To make the comparison between the open clusters' and the moving groups' age and metallicity more quantitative, we show in Figure 4 a comparison between the observed parallaxes of the moving group members and the predicted parallaxes based on the open clusters' isochrone and the observed photometry for each main-sequence star in the sample; this comparison is similar to the one performed by Famaey et al. (2008). That is, using the observed color of a star and the M_V versus $B-V$ relation corresponding to the isochrone of the associated open cluster we predict the absolute magnitude of the star and convert this to a model parallax using the observed apparent V magnitude. Conservatively, we do not consider any star for which we cannot obtain a photometric parallax in this way, for example, because its color is inconsistent with the age and metallicity of the cluster; if any such stars is a high-probability member of the moving group, this star alone rules out the open-cluster origin of the moving group. In order to compute the photometric parallax we use, for each moving group, the first of the isochrones mentioned in the caption of Figure 3; the results for the second set of isochrones are very similar to the ones presented below. In each of the histograms all of the main-sequence stars of the sample are plotted; their contributions to each histogram are weighted by their probabilities of being members of the moving group in question, as calculated in Section 2.2.

Two different comparisons between the observed parallaxes and the model parallaxes are shown in Figure 4. The left histogram shows the distribution of observed and model parallaxes for each moving group. Although the effect of parallax uncertainties (typically $\sim$1 mas) is not included in this comparison, a clear offset between the observed and model parallaxes can be seen. For each moving group, the hypothesis that the moving group originated from the open cluster systematically underestimates the distance to each star. This effect is made even more apparent in the right figure of each of the panels. Shown here is the distribution of the difference between the observed and the predicted parallaxes, normalized using the observational uncertainty on the parallax. If the single-burst stellar population corresponding to the open-cluster explanation for the moving groups were correct, this histogram should be that of a Gaussian distribution of mean zero and standard deviation 1. However, it is immediately clear that the distribution is much broader than this expected Gaussian, and that it is significantly skewed. This skewness corresponds to the systematic offsets between model and observations discussed above. As we will argue now, it is this excessive skewness, rather than the excessive width, of this

[4] Retrieved using the Web interface provided by Leo Girardi at the Astronomical Observatory of Padua, http://stev.oapd.inaf.it/cgi-bin/cmd_2.2.

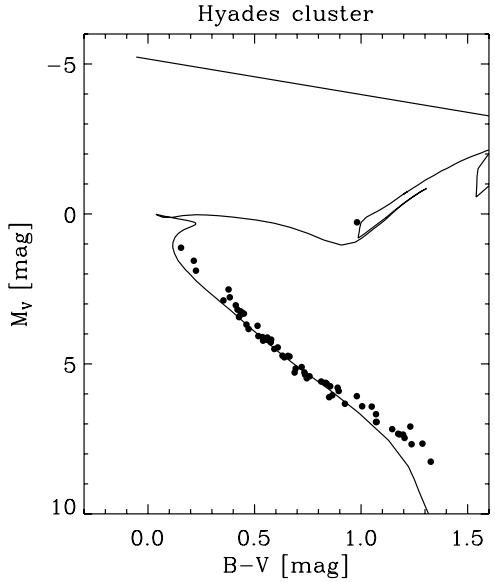

Figure 5. Color–magnitude diagram of the Hyades cluster with the 625 Myr, $Z = 0.019$ isochrone overlaid. These members are selected from the catalog of Hyades members compiled by Perryman et al. (1998): we selected those stars that have a final membership entry "1," that are single, and that lie within 10 pc of the center of the Hyades cluster.

distribution that shows that the moving groups cannot be fully explained as being part of the evaporation of their eponymous open clusters.

The reason why it is dangerous to attach too much significance to the much larger-than-expected width of the parallax residual distribution is because even the associated open clusters have a small amount of scatter in their age and metallicity properties that has not been taken into account here and this scatter would have to be added to the variance of the expected Gaussian to see whether the model is a good fit. This fact is illustrated in Figures 5 and 6. Shown here are figures similar to Figures 3 and 4 but for the Hyades cluster. We have taken a list of probable Hyades cluster members in the *Hipparcos* catalog from Table 2 of Perryman et al. (1998): we only select those stars that have a final membership entry "1," that are single, and that lie within 10 pc of the center of the Hyades cluster. This procedure selects 61 Hyades members. The color–magnitude diagram of these stars is shown in Figure 5 with the 625 Myr, $Z = 0.019$ isochrone overlaid. The Hyades members hug the isochrone closely, especially in the range 0.4 mag $< B - V <$ 0.9 mag. The correspondence between the isochrone and the members' color and magnitude becomes less good for redder stars at $B - V > 1.0$ mag; the reason for this is unclear, since the color–magnitude diagrams with best-fit isochrones do not extend this far redward in Perryman et al. (1998), but it might be related to subtle effects in the calculation of the theoretical isochrones. As expected, there is no sign of a large, systematic offset between the theoretical isochrone and the observed color–magnitude relation. Note that most Hyades open cluster members considered here are high-probability members of the Hyades moving group: all but 15 of the stars are above the $p_{ij} = 0.4$ threshold that gives an overall level of moving-group structure in the velocity distribution comparable to the observed level (see below); 39 of the stars even have membership probabilities larger than 0.7. Thus, if all high-probability members of the moving groups studied in this section were as consistent with a single-burst stellar population as the

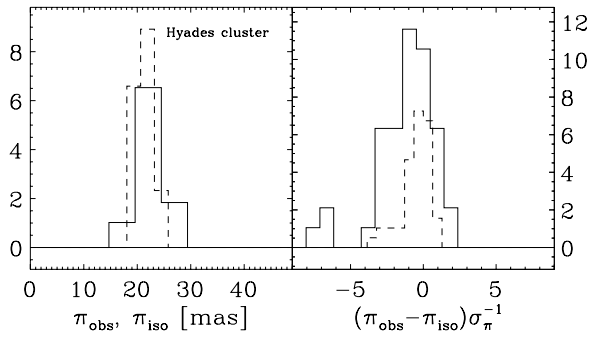

Figure 6. Same as Figure 4 but for the Hyades cluster of Figure 5. The dashed histogram in the right panel is what one gets after adding a 0.2 mag spread in quadrature to the observational uncertainty in the parallax (this histogram has been scaled down by a factor of 3 for display purposes).

Hyades open cluster, we would expect to detect this by our procedure.

Figure 6 shows for the Hyades cluster the same histograms presented in Figure 4 for the moving groups. The observed distribution of parallaxes and the distribution of model parallaxes for the Hyades members, again calculated using the Hyades isochrone and the observed photometry for the stars, are very similar and no systematic difference such as the one observed for the moving groups in Figure 4 can be seen. This is confirmed in the right panel of Figure 6 where the histogram of the normalized difference between observed and model parallaxes is shown for the 61 Hyades members. While this distribution peaks at zero, indicating that there is no systematic bias in the model parallaxes, the distribution is broader than the expected standard-deviation-one Gaussian distribution. This indicates that the scatter in the age and metallicity of the Hyades members produces a scatter in the model parallaxes that should be taken into account in the model comparison above. The distribution in the right panel also exhibits a small amount of skewness and heavy-tailed behavior. However, this skewness is small and simply related to the departure from the isochrone of the stars redward of $B-V = 1.0$ mag; there is no indication of the smooth skewness and heavy tail seen in Figure 4. Thus, while the breadth of the model comparison histograms in the right panels of Figure 4 does not provide a convincing reason to reject the open cluster origin of the moving groups, the large amount of skewness and the heavy tails in these distributions clearly indicates that the model of the moving groups being evaporating parts of their eponymous open clusters is not a good fit to the moving-group photometric properties. We can safely say that the kinematically identified, low-velocity, moving groups do not appear to have the same stellar population as the open clusters after which they are named.

One might worry about the influence of the very low probability ($p_{ij} < 0.1$) and/or the red ($B - V > 0.9$ mag)—because of the discrepancy between the model isochrone and the observed absolute magnitudes of these stars for the Hyades cluster discussed above—moving group members in the discussion above. We have therefore repeated the previous analysis leaving out stars from the sample which satisfy either of these two criteria. The histograms obtained in this way are barely distinguishable from the distributions shown in Figure 4 and the argument made in the previous paragraphs continues to hold.

4. STRATEGY FOR THE SECOND PART OF THIS PAPER

Even though we have shown that the moving groups cannot be considered to be the evaporating parts of their associated

open clusters, the question still remains whether they can be considered to be some single-burst stellar population, perhaps originating from an open cluster that has completely evaporated and thus has no presently identifiable core. It might be that it is merely a coincidence that the kinematically defined moving groups' space velocities roughly coincide with those of prominent open clusters, while the moving groups are actually remnants of older open clusters that are hard to identify at the present day. We have also failed to explain the origin of the Hercules moving group in the previous section because of the lack of an associated open cluster. Therefore, in what follows we will test the hypothesis that the low-velocity moving groups each comprise *some* single-burst stellar population, with an a priori unknown age and metallicity. If the moving groups fail to live up to this hypothesis, we can confidently say that they are not remnants of inhomogeneous star formation, but instead most likely have a dynamical origin.

Hypothesis testing or model selection is at its strongest when two mutually exclusive hypotheses can be pitted against each other as opposed to merely testing whether a particular hypothesis provides a good fit to the data. Fortunately, we are in a situation here in which there is a well-specified background hypothesis: this hypothesis is simply that the stars in the moving groups are nothing more than a sparse sampling of the full locally observed disk population, that is, that there is nothing special about their age and chemical composition to distinguish them from local disk stars as a whole. We are also lucky to have a non-parametric model at our disposal for this background hypothesis: this model is nothing more than the observed local population of disk stars. Thus, we can test whether the moving groups' photometric properties are better described by the model in which each contains just a single-burst stellar population or by the model in which each contains just the same population as the background stars. The single-burst stellar population model can make very tight predictions for the photometric properties of the stars, while the background model can only make very broad statements about the moving groups' member properties. If the tight predictions play out, this will lead to clear evidence of the evaporating-cluster nature of the moving groups because the photometric properties of the member stars will be much more probable than they are under the background hypothesis. However, if the single-burst stellar population hypothesis fails to predict the photometric properties of the moving group members, then the background model will be preferred. This conceptual view of the model selection procedure which we will use in the second part of this paper is illustrated in Figure 7.

Coupled with an initial mass function, the age and metallicity of a single-burst stellar population imply a density, or distribution, in the color–magnitude plane, and testing whether a population of stars consists of a single stellar population is equivalent to checking whether the observed distribution of stars in the color–magnitude plane is consistent with this density. This is a very strict test of the coeval hypothesis that depends on choosing, or inferring, the right initial mass function and having complete samples of stars at one's disposal. A more conservative approach, which does not rely on these two assumptions, would be to test whether the relation between color and absolute magnitude predicted for a coeval population of a certain age and metallicity is observed in the sample. That is, rather than testing whether the predicted density is observed in the color–magnitude plane of a sample of stars, we test whether the predicted regression $M_V(B-V)$ is consistent with the data. In practice, we use the predicted $M_V(B-V)$ relation combined

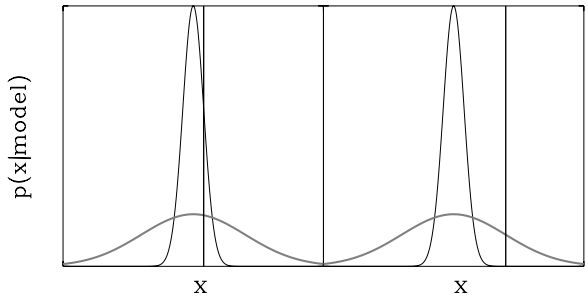

Figure 7. Model selection: the *y*-axis represents the probability of measuring the value on the *x*-axis for a foreground model (thin, black curve) and a background model (thick, gray curve). The foreground model makes very informative predictions while the broader background model makes less informative predictions. Therefore, when both the foreground model and the background model predict the right observed value (vertical line) the observed value has a larger probability for the foreground model (left panel); when the foreground model fails to predict the observed value, the observed value is more probable under the background model (right panel).

with the observed photometry of a star to predict a photometric parallax for the star, in exactly the way described in the previous section. This photometric parallax is then compared to the observed parallax, taking into account the observational uncertainty on the parallax.

For the hypothesis that we are interested in testing this is advisable because mass segregation and selective evaporation have been shown to affect the luminosity functions of open clusters, both in simulations (Aarseth & Woolf 1972; Terlevich 1987; de la Fuente Marcos 1995; Bonnell & Davies 1998)—whether primordial (Bonnell & Davies 1998; Hillenbrand & Hartmann 1998) or dynamical (McMillan et al. 2007; Moeckel & Bonnell 2009; Allison et al. 2009)—as well as observationally in some of the open clusters associated with the moving groups studied here (Hyades: Reid 1992; Perryman et al. 1998; Reid & Hawley 1999; Dobbie et al. 2002; Bouvier et al. 2008; Pleiades: Bouvier et al. 1998; Hambly et al. 1999; Adams et al. 2001; NGC 1901: Carraro et al. 2007). There is some debate about whether mass segregation has actually been observed in massive open clusters (Ascenso et al. 2009). We can expect low-mass stars to be preferentially ejected from open clusters, although quantitative estimates of this effect are still highly uncertain. It would be hard to predict the complete two-dimensional model density in the color–magnitude plane. However, whether or not selective evaporation plays a large role in the evolution and evaporation of open clusters, the relation $M_V(B-V)$ should always hold if the sample of stars originated from a single star formation event and the model selection test based on it will not be affected.

The test will hinge on the existence of a background model that states that the stars in the moving groups are similar to the local disk population as a whole. In the next section, we will refine this background model and put it in such a form that we can use it quantitatively in the model selection test. That is, we will turn the bulk photometric properties of the local disk stars in *Hipparcos* into a photometric parallax relation—predicted model parallax plus model scatter—which can be compared to the photometric parallax obtained for a single-burst stellar population for each star.

5. THE BACKGROUND MODEL

Given that we have at our disposal a large number of stars with accurate photometry and parallaxes to estimate a one-dimensional photometric parallax relation, it is unlikely that

any parametric model could capture the observed relation and its scatter in all of its details. It is, therefore, advisable to use a non-parametric approach to estimate the photometric parallax relation and its intrinsic scatter for the background population. Principled probabilistic approaches to this exist (e.g., using Gaussian process regression; Rasmussen & Williams 2006) but given the low-dimensional nature of the problem and the large amount of data—from Figure 2 it is clear that at most points there are at least dozens of stars with which to estimate the local relation—we can expect simpler procedures to perform adequately.

To constrain the background model we use all of the 15,023 stars in our *Hipparcos* sample. Strictly speaking, we are testing whether one or more of the moving groups is distinct from the local disk population of stars in that it consists solely of stars of a narrow age and metallicity range, and therefore, including these moving group members in the background model mixes into the background model the stellar populations of the moving groups. This could complicate model selection, since it will be harder to distinguish between the background and the foreground models (for the purposes of this section and the next, the foreground model for each moving group is that it is a single-burst stellar population) when the background model is more like the foreground model than it should be. In principle, we should test each combination of moving-group/not-a-moving-group for each of the moving groups and build background models out of stars that are not believed to be part of a single-burst stellar population in that particular model selection test. This would be impractical, not in the least because few of the stars can be confidently assigned to a specific moving group or even background, and making subsamples would necessarily involve making hard cuts on membership probabilities, with all of the biases that would result from that. We therefore use all of the stars to construct the background model and investigate each moving group separately in the following by testing against this background model. Given that more than 60% of the stars are believed to be part of the background (see BHR) and that the population of moving groups taken together would presumably span some range of age and metallicity, the effect of including real moving group members in the background sample should be small. It is important to note, however, that even if the moving groups significantly affect the background model, this will only bring the foreground and the background model closer together, but the foreground model should still be preferred over the background model when the moving group is a single-burst stellar population.

From our sample of 15,023 main-sequence stars, we construct a non-parametric photometric parallax relation: for each star i we take the stars in our *Hipparcos* sample in a small color bin (see below) around star i's color and consider the absolute magnitudes of the stars in this color bin to represent the complete set of absolute magnitudes that a star in this color bin could have, that is, the probability of the absolute magnitude of star i is given by

$$p(M_{V,i}|(B-V)_i) = \sum_{\substack{j \\ (B-V)_j \approx (B-V)_i}} \delta(M_{V,i} - M_{V,j}), \quad (3)$$

where $\delta(\cdot)$ is the Dirac delta function. The exact meaning and implementation of $(B-V)_j \approx (B-V)_i$ are discussed in detail below. Given this finite set of possible absolute magnitudes for star i, we use the observed V magnitude of star i to derive a probability estimate for its parallax π_i, that is,

$$p(\pi_i|V_i, M_V) = \delta(\pi_i - \pi[V_i, M_V]), \quad (4)$$

$$\pi[V, M_V] = 10^{[(M_V - V)/5+2]}, \quad (5)$$

$$p(\pi_i|V_i, (B-V)_i) = \sum_{\substack{j \\ (B-V)_j \approx (B-V)_i}} \delta(\pi_i - \pi[V_i, M_{V,j}]), \quad (6)$$

where $[\pi] =$ mas. To define the notion of "nearness," that is, the implementation of $(B-V)_j \approx (B-V)_i$ in the expressions above, we use the concept of a kernel (in this sense the method described here is similar to that of a linear smoother in non-parametric statistics; Wasserman 2005). Using a kernel $w(\cdot; \lambda)$ we define a distance between two colors $x_i \equiv (B-V)_i$ and $x_j \equiv (B-V)_j$ as $w(x_i - x_j; \lambda)$, where λ is a width parameter of the kernel, and we use this notion of distance to weight the contributions of the various stars in the background sample. These weights are inserted into Equation (3) as follows:

$$p(M_{V,i}|(B-V)_i) = \frac{1}{W} \sum_j w(x_i - x_j; \lambda)\, \delta(M_{V,i} - M_{V,j}), \quad (7)$$

where x_i and x_j are the colors of the stars and W is a normalization factor equal to $\sum_j w(x_i - x_j; \lambda)$. To compare this photometric parallax with the observed trigonometric parallax $\pi_{\mathrm{obs},i}$ we convolve this distribution with the observational uncertainty $\sigma_{\pi,i}$, assumed Gaussian:

$$p(\pi_{\mathrm{obs},i}|\sigma_{\pi,i}, V_i, (B-V)_i) = \frac{1}{W} \sum_j w(x_i - x_j; \lambda) \times \mathcal{N}\left(\pi_{\mathrm{obs},i}|\pi[V_i, M_{V,j}], \sigma^2_{\pi,i}\right), \quad (8)$$

where $\mathcal{N}(\cdot)$ is the normalized, one-dimensional Gaussian distribution and $\pi[V, M_V]$ is given by Equation (5). The probability distributions for the observed parallax obtained in this way are shown for a random sample of stars in Figure 8 together with the actual observed value of the trigonometric parallax (the kernel and its width used in this figure are the optimal ones for the background model as discussed below).

Several considerations play a role in choosing a kernel function $w(\cdot; \lambda)$. On the one hand, one wants a kernel that is as smooth as possible, smoothly going from giving high weights to points that are close in color space to low weights for stars on the other side of the main sequence. However, it is computationally advantageous to use a kernel that has a finite support such that in constructing the photometric parallax prediction in Equation (8) only a subset of the 15,023 in the whole sample are used. For this reason, a Gaussian kernel

$$w(u; \lambda) = \exp\left(-\frac{u^2}{2\lambda^2}\right), \quad (9)$$

while smooth, is unwieldy. Therefore, we have considered the following finite-range kernels: the Tricube kernel

$$w(u; \lambda) = \left(1 - \left(\frac{u}{\lambda}\right)^3\right)^3, \quad u \leqslant \lambda, \quad (10)$$

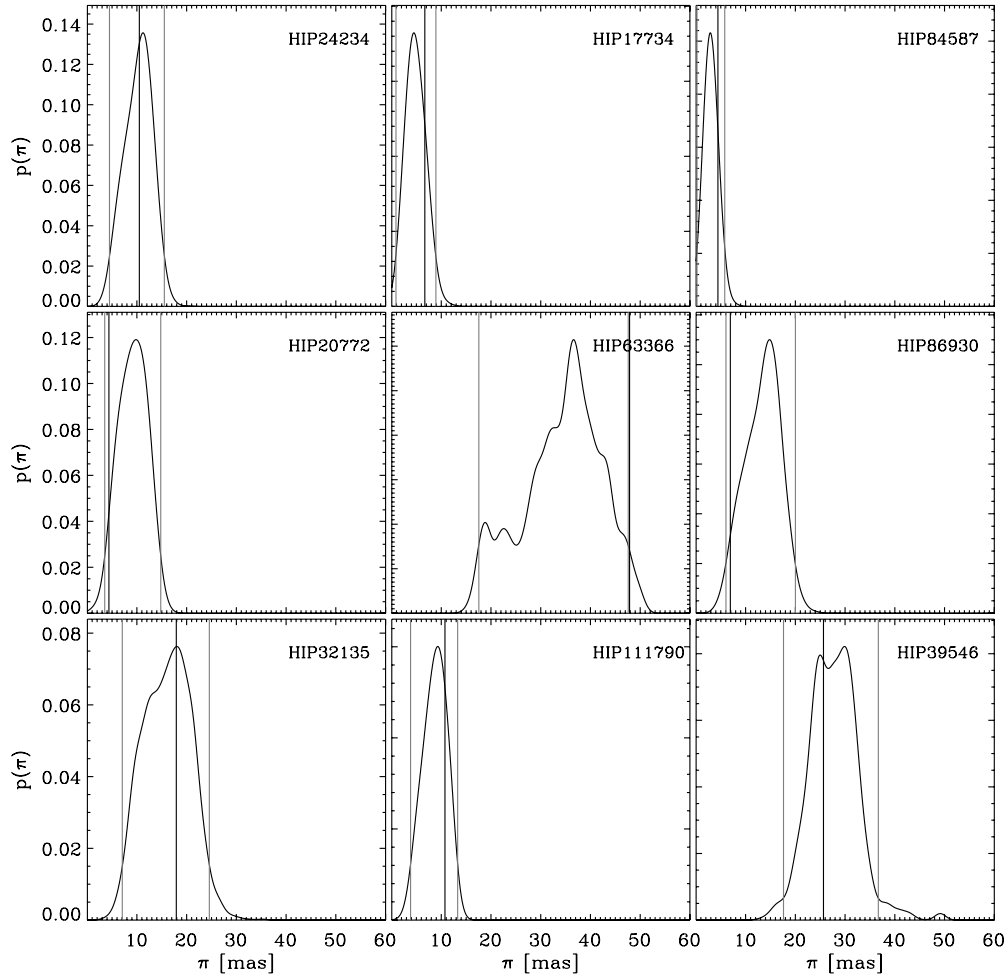

Figure 8. Background model predictions for the parallax of nine random stars in the basic *Hipparcos* sample. The background model consists of a linear smoother with a Tricube kernel with width parameter $\lambda = 0.05$. In each panel, the background model has been convolved with the observational parallax uncertainty. The observed parallax (thick, black line) as well as 95% confidence regions (thin, gray lines) are indicated.

and the Epanechnikov kernel

$$w(u;\lambda) = \left(1 - \left(\frac{u}{\lambda}\right)^2\right), \quad u \leqslant \lambda\,. \tag{11}$$

Of these, the Tricube kernel is everywhere differentiable; it combines the best of both worlds.

Each of the kernels has a width parameter λ that is unknown a priori. We need to train the background model, i.e., establish a good value of λ. We train the background model using leave-one-out cross-validation (Stone 1974): for each choice of the width parameter λ on a logarithmically spaced grid in λ, we compute the probability of each of the observed parallaxes in our sample using as the training $\{B - V, M_V\}$-set all of the other stars in our sample. We then multiply the probabilities thus obtained for all of the stars and take the logarithm of this product to compute the "score" for that value of λ; this quantity is also known as the "pseudo-likelihood." The value of λ with the highest score is the preferred value of λ.

We computed the cross-validation score for a range of values of λ for each of the kernels; these are shown in Figure 9. It is clear that all three kernels agree on the best value of λ (keeping in mind that the Gaussian kernel has infinite range and only approaches zero for $u > 2\lambda$). As expected, the resulting cross-validation score curve for the Gaussian kernel is much smoother than the corresponding curves for the Tricube and Epanechnikov kernels and the maximum score for the Gaussian kernel is somewhat higher than that for the Tricube kernel, but because computations with the Gaussian kernel are much slower and the gain in performance is small, we choose the Tricube kernel for the background model. This is, again, a conservative choice, since a slightly worse background fit can only make it easier for the foreground model to be preferred. All three kernels agree that the optimal width is approximately $\lambda = 0.05$ mag and this is the value used in the background model.

To test whether the background model with the chosen kernel parameters actually provides a good fit to the data or whether it is merely the best possible fit among the possibilities explored (note that we do not expect this to be the case as this is a non-parametric model), we have checked whether the background-model parallax probability distribution in Equation (8) is a consistent description of the parallax distribution in that all of the quantiles of the distribution are correct. Figure 10 shows the distribution of the quantiles of the parallax distribution at which the observed, trigonometric parallaxes are found. If the background model is a good description of the observed parallaxes, then this distribution should be uniform. That is, if Equation (8) correctly predicts the 95% confidence interval, the 90% interval, and so on, then the background model is a good fit to the data. The distribution in Figure 10 is flat over most of the range between 0 and 1, with the only major deviations near the edges of this interval, and we can therefore say that the

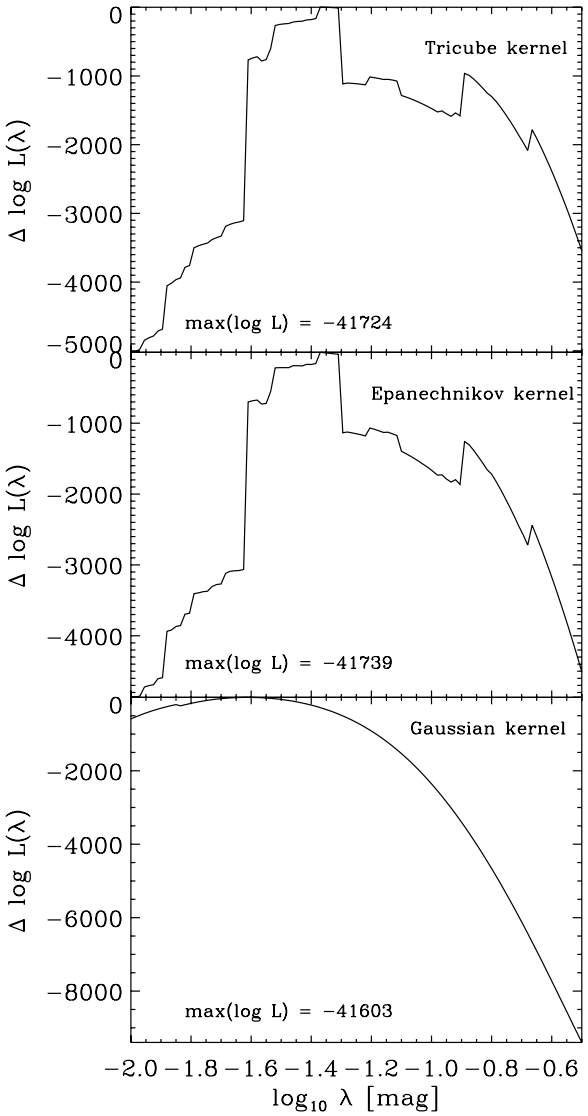

Figure 9. Selection of the width parameter λ of the kernel used in the kernel-regression background model.

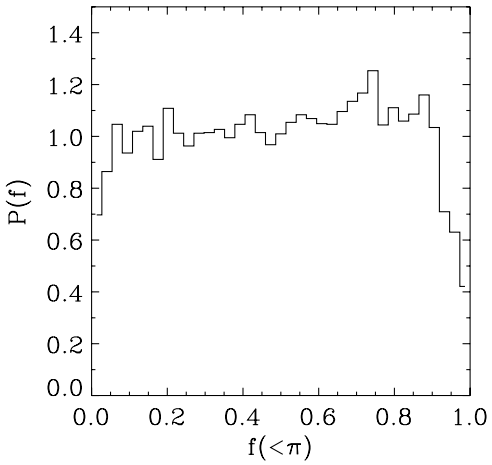

Figure 10. Distribution of the quantiles at which the observed parallax is found of the background-model predictive distribution for the parallax. This curve should be flat for perfectly consistent predictive distributions—meaning that they correctly predict all of the quantiles of the distribution.

background model provides a good fit to the bulk of the data. That the background model fails for stars at the edges of the parallax distribution is not surprising as these are rare: nearby and faint or distant and bright stars are sparsely sampled regions of the color–magnitude diagram in a magnitude-limited sample as is clear from Figure 2.

6. THE MOVING GROUPS ARE NOT SINGLE-BURST STELLAR POPULATIONS

The goal of this section is to establish whether the moving groups could conceivably arise from an evaporating cluster, or whether their stellar content is inconsistent with being produced by a single burst of star formation. We will fit a model of a single-burst stellar population to each of the five moving groups and test whether this model is a better fit to the moving-groups data than the background model described in the previous section. The foreground hypothesis for the purpose of this section is therefore that the moving group is characterized by a single age and metallicity.

Like the background model, the foreground model defines a photometric parallax relation. While that defined by the background sample is a broad model, roughly consisting of a mean photometric parallax relation and a large amount of scatter around this mean, the foreground model's photometric parallax relation is very narrow, or informative, in that it is given by the single isochrone corresponding to an assumed age and metallicity (single in the sense of being the unique isochrone in the Padova database), smoothed by the observational uncertainty. The probability of an observed, trigonometric parallax $\pi_{\mathrm{obs},i}$ assuming a certain age and metallicity Z, and given the star's color $(B-V)_i$, apparent magnitude V_i, and observational uncertainty, $\sigma_{\pi,i}$, is given by

$$p(\pi_{\mathrm{obs},i}|\mathrm{Age}, Z, \sigma_{\pi,i}, V_i, (B-V)_i) = \mathcal{N}\left(\pi_{\mathrm{obs},i}|\pi[V_i, (B-V)_i, \mathrm{Age}, Z], \sigma^2_{\pi,i}\right), \quad (12)$$

where the photometric parallax $\pi[V_i, (B-V)_i, \mathrm{Age}, Z]$ is derived from the isochrone absolute magnitude as in Equation (5). The absolute magnitude is derived from the isochrone by reading off the absolute magnitude along the isochrone corresponding to the assumed age and metallicity at the star's observed color $(B-V)_i$.

Equation (12) is not the whole story. First, Figures 5 and 6 show that even an open cluster itself is not perfectly fit by a single isochrone, that is, the right histogram in Figure 6 is much broader than the unit variance Gaussian distribution. We find that there is 0.2 mag of root variance in absolute magnitude with respect to the isochrone locus of the stars in Figure 5. We propagate this to a variance in the parallaxes of the Hyades cluster members and add it in quadrature to the observational parallax uncertainty. The resulting photometric parallax–observed parallax comparison is also shown in Figure 6 as the dashed histogram. This distribution has close to unit variance; the open-cluster scenario now provides a good fit to the data (this procedure is somewhat equivalent to adding a small amount of unmodeled noise or "jitter").

Second, the assumption of a certain age and metallicity for a moving group is too easily falsified. When we observe a star that is a member of a moving group, but that has a color that is inconsistent with that age and metallicity, e.g., because the star is too young to still be on the main sequence of an old population of stars, this combination of age and metallicity is ruled out by the existence of this single star alone. As useful as the idea of falsification has been in epistemology, and as helpful

as it could be in this case if we had high-probability members of the moving groups in our sample, the ease of falsification is actually problematic since we cannot confidently assign any of the stars in our sample to moving groups and we need to take the odds that a star is in fact a background interloper into account. The proper way to take this interloper's probability into account is to divide the probability of a star's properties among the foreground and background hypotheses in a way that is proportional to the probability that the star is part of the moving group or not. Thus, we write the probability of the observed parallax of each star as

$$p(\pi_{\mathrm{obs},i}) = p(\pi_{\mathrm{obs},i}|\mathrm{foreground})^{p_{ij}}\; p(\pi_{\mathrm{obs},i}|\mathrm{background})^{1-p_{ij}}\,, \tag{13}$$

where p_{ij} is the probability that star i is a member of moving group j; see Equation (2). A low-probability member of a moving group, one that is most likely *not* a member, has the bad property that it can rule out a certain age and metallicity due to its color being inconsistent with it, since the first factor in Equation (13) will be zero for any non-zero p_{ij} and the probability of an age and metallicity of a moving group is given by Bayes's theorem

$$p(\mathrm{Age},\, Z|\{\pi_{\mathrm{obs},i}\}) \propto p(\mathrm{Age},\, Z)\prod_i p(\pi_{\mathrm{obs},i}|\mathrm{Age},\, Z)\,, \tag{14}$$

where we have implicitly assumed the other observational properties of the star (i.e., its color, apparent magnitude, and observational parallax uncertainty) in the conditional probabilities. A single star with a color that is inconsistent with the age and metallicity under investigation for the moving group therefore rules out this age and metallicity, as it factors in a zero probability in the product in Equation (14).

Instead of just using the isochrone prediction in evaluating the probability of an observed parallax under the foreground model in Equation (12), we add a small contribution from the background into the probability, such that the first factor in Equation (13) becomes

$$\begin{aligned} p(\pi_{\mathrm{obs},i}|\mathrm{foreground}) = {} & (1-\alpha)\; p(\pi_{\mathrm{obs},i}|\mathrm{Age},\, Z) \\ & + \alpha p(\pi_{\mathrm{obs},i}|\mathrm{background})\,, \end{aligned} \tag{15}$$

where the background probability is given by Equation (8). The parameter α is, in general, a free parameter and is a measure of the amount of background contamination. The total foreground probability is obtained by substituting this equation into Equation (13). A star whose color is inconsistent with an assumed age and metallicity will now automatically resort to its background probability, since then $p(\pi_{\mathrm{obs},i}|\mathrm{Age},\, Z)$ is zero and

$$\begin{aligned} p(\pi_{\mathrm{obs},i}|\mathrm{foreground}) = {} & [(1-\alpha)\; p(\pi_{\mathrm{obs},i}|\mathrm{Age},\, Z) \\ & + \alpha p(\pi_{\mathrm{obs},i}|\mathrm{background})]^{p_{ij}} \\ & \times p(\pi_{\mathrm{obs},i}|\mathrm{background})^{1-p_{ij}} \\ = {} & \alpha^{p_{ij}}\, p(\pi_{\mathrm{obs},i}|\mathrm{background})\,. \end{aligned} \tag{16}$$

Low-probability members have $p_{ij} \approx 0$ such that $\alpha^{p_{ij}} \approx 1$. This expression shows that when α is a free parameter, it will be advantageous to make it large when high-probability members are inconsistent with the assumed age and metallicity, to make the fit at least as good as the background fit.

When α is allowed to take any value between 0 and 1, it is clear that if the fit prefers a value of α that is close to 1, this will be an indication that the single-burst stellar population model is not a very good fit to the moving-group data. But what value of α do we expect if the data are consistent with the moving group having originated from a single burst of star formation? In order to answer this question, we look at the overall properties of the velocity distribution. We look at the fraction of stars in one of the moving groups as a function of a hard cut on the membership probabilities p_{ij} to assign moving-group members. We find that a hard cut of $p_{ij} > 0.4$ gives rise to a fraction of moving-group substructure consistent with the overall fraction of the substructure observed in the velocity distribution, i.e., 40%. We can then ask: what is the accumulated fraction of membership probability of stars with membership probabilities less than this hard cut? This gives an estimate of the background contamination for each moving group, that is, it gives an indication of the influence of the background stars on inferences using the membership probabilities. These background contamination levels α are given in Table 1 on the first line for each moving group.

Table 1
Best-fit Single-stellar-population Models for the Low-velocity Moving Groups

Group	Age (Myr)	Z	α[a]
NGC 1901	180	0.030	0.41
NGC 1901	56	0.030	0.98
Sirius	350	0.026	0.53
Sirius	413	0.023	0.90
Pleiades	67	0.030	0.57
Pleiades	67	0.030	0.90
Hyades	488	0.029	0.58
Hyades	679	0.027	0.86
Hercules	180	0.030	0.83
Hercules	180	0.030	1.00

Notes. The first line for each group lists the best-fit age and metallicity for the fixed value for α in the last column—this value was obtained from a global contamination analysis (see the text)—the second line lists the overall best-fit age, metallicity, and α.
[a] Background contamination level.

If we allow the fit to vary the background contamination level α and we find that the fit prefers values of α that are much larger than the value of α estimated for each moving group from the global analysis described above, that is a strong indication that the moving groups are not single-burst stellar populations. This does not rule out that certain parts of the moving group are consistent with being created in a single burst—a preferred value of α that is close to but not equal to unity could suggest this. Therefore, we perform two fits: one in which we fix α at the value determined in the last paragraph and the other in which we allow α to take on any value between 0 and 1. In both cases, we vary the age and metallicity of the underlying isochrone on a grid in log age and metallicity space. The best fit is then given by the combination of age, metallicity, and—if left free—α that maximizes the probability of the foreground model in

$$p(\log \mathrm{Age},\, Z(,\alpha)) \propto \prod_i p(\pi_{\mathrm{obs},i}|\,\log \mathrm{Age},\, Z(,\alpha))\,, \tag{17}$$

where the individual conditional probabilities are given by Equation (13) and the parentheses around α indicate that we either fix α or vary it. This is a maximum-likelihood fit or, equivalently but relevant in what follows, the maximum of the posterior probability distribution for age, metallicity, and

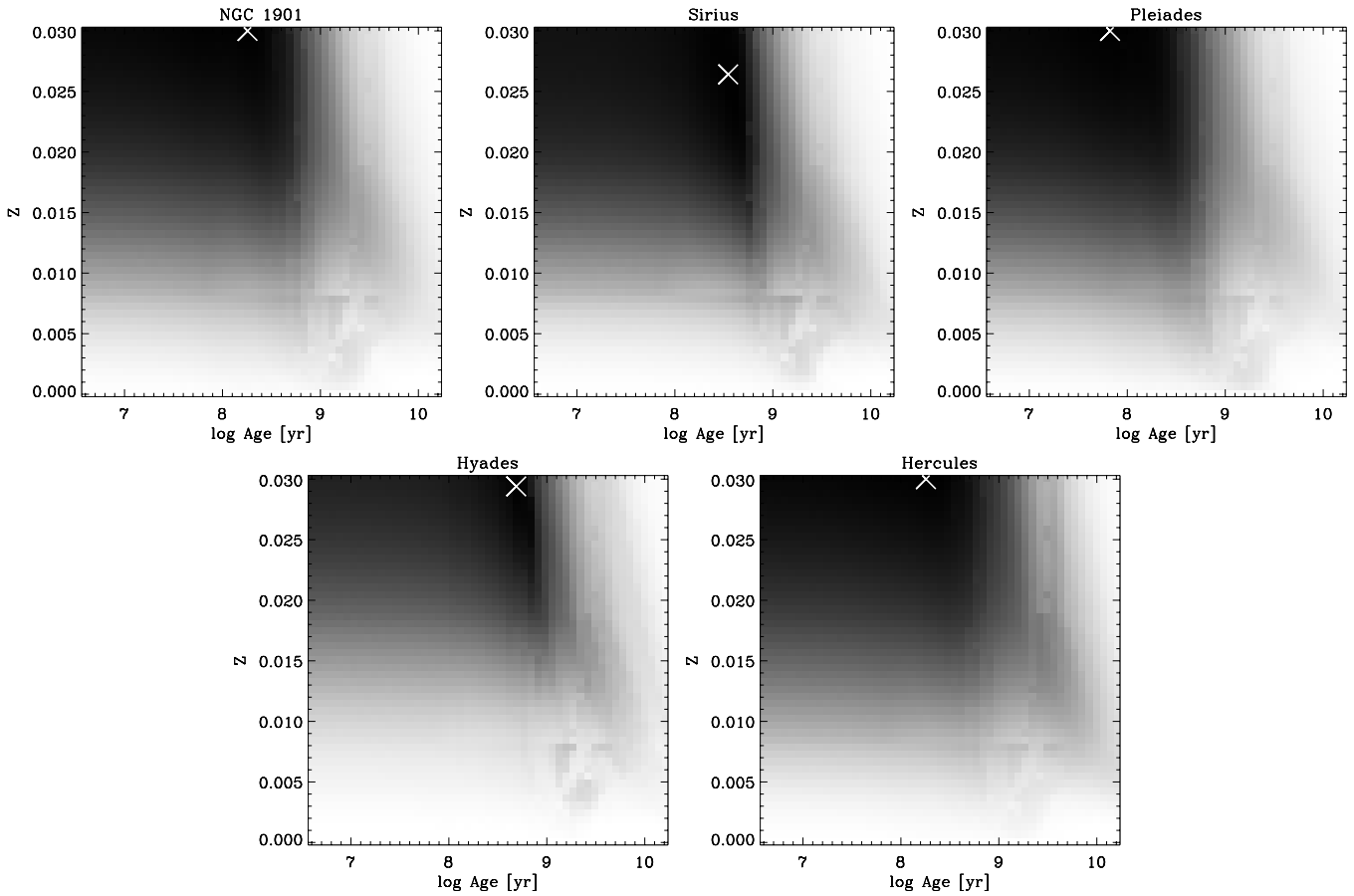

Figure 11. Logarithm of the likelihood of different single-burst stellar population models characterized by an age and metallicity Z for the low-velocity moving groups, with the background contamination level α for each group set to the value obtained from a global contamination analysis (see the text). The best-fit model is indicated by a white cross.

α with uniform priors on log age, metallicity, and α. The latter attitude permits marginalization over subsets of the parameters. In performing the fit, the last factor in Equation (13) is irrelevant, as it does not depend on any of the fit parameters, but in the model selection it does need to be taken into account.

The results of this fit when fixing α are shown in Figure 11 for each of the five moving groups. The logarithm of the expression in Equation (17) (up to an arbitrary normalization term) is shown and the best-fit value of age and metallicity is indicated. These best-fit values are given in Table 1 on the first line for each moving group. For the moving groups with an associated open cluster the best-fit ages are similar to those of the open clusters, but the metallicities are very different. This confirms the result from Section 3 that the moving groups are not made up of former open cluster members. The posterior distribution for age and metallicity is rather broad for all of the moving groups, indicating that there is no clear preference for a specific age and metallicity. Given the amount of data on each moving group—each moving group has a weight of about 10% in the full velocity distribution, translating into about 1000–1500 stars in our sample—this is another indication that the moving groups contain more than a single stellar population.

When allowing the background contamination parameter α to be fit as well, the best-fit ages and metallicities are similar to those obtained for fixed α, but the parameter α is drawn to values close to unity. The posterior distribution for the age and the metallicity, marginalized over α using a uniform prior on α, is shown in Figure 12; the posterior distribution for α, likewise marginalized over the logarithm of the age and the metallicity, is shown in Figure 13. The best-fit values are listed in Table 1 on the second line for each moving group. It is clear from these results that the best-fit level of background contamination is very high for each of the moving groups; for Hercules, the best-fit value of α is actually equal to unity. Especially in the marginalized distributions for α—our degree of belief concerning α given that we believe that part of the moving group was produced in a single burst of star formation without caring about the age and metallicity of that event—the peak of the distribution is at large values of α and even at $\alpha = 1$ for the NGC 1901 and Hyades moving groups, and in all cases much higher than the expected level of background contamination indicated by the vertical line. This tells us that most of each moving group, if not all of it, is better fit by the background than by any single-burst stellar population.

Although it is telling that the background contamination level in each moving group, if left as a free parameter in the fit, is drawn to high levels of contamination, we will take our hypothesis testing one step further by examining which of the two hypotheses for each moving group, i.e., that it is an evaporating cluster or that it is merely a sparse sampling of the background population of stars, is better at predicting the properties of an external data set. As this external data set we use the stars in the GCS sample (Nordström et al. 2004), which consists of a subset of the *Hipparcos* data set with additional radial velocities. We select stars that are not suspected to be giants or to be part of a binary in exactly the same way as

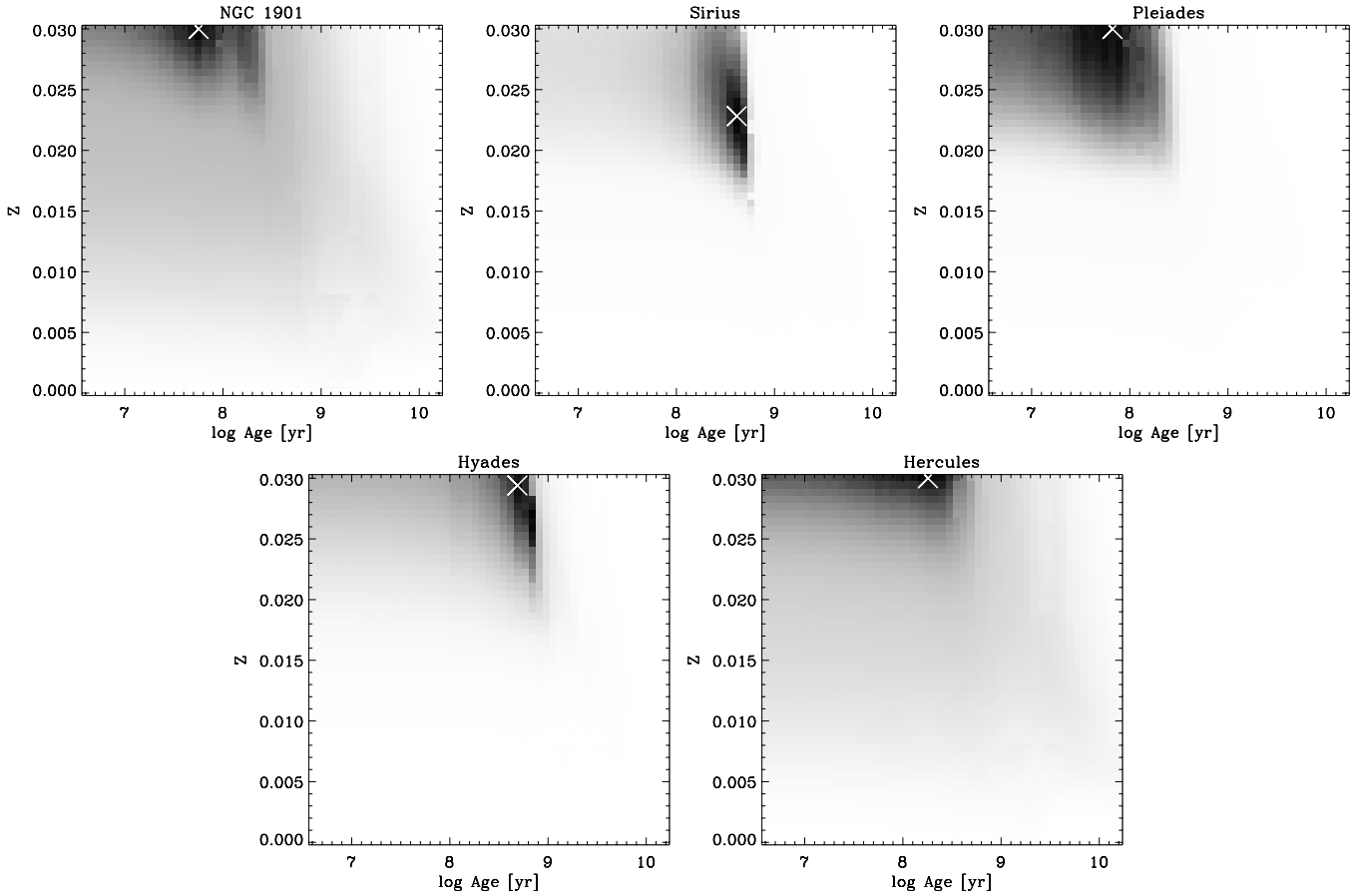

Figure 12. Logarithm of the likelihood of different single stellar population models characterized by an age and metallicity Z for the low-velocity moving groups, marginalized over the background contamination level α with a uniform prior on α. The best-fit model is indicated by a white cross.

described in Section 2.4 in BHR. At this point, we only take the radial velocities of this sample of 7682 stars, consulting the revised *Hipparcos* catalog (van Leeuwen 2007) for all of the other properties of these stars. This sample of stars contains stars that are in the basic *Hipparcos* sample that we used before to fit the age and metallicity of the moving groups and that we used to construct the background model as well. The trigonometric parallaxes are therefore *not* an entirely independent sample of parallaxes. But the GCS sample is completely external in the following sense: we can use the radial velocities from the GCS catalog to calculate the membership probabilities p_{ij} for all of the stars in the GCS sample in a similar way as in Equation (2) but with $\mathbf{R}_i$ now the projection onto the line-of-sight direction. This way of assigning membership probabilities is independent of the way we assigned membership probabilities before, since those were calculated using the tangential velocities. It is in this sense that the GCS data set is external; in what follows, we will determine whether the foreground model trained on the basic *Hipparcos* sample using tangential velocities predicts the properties of the moving group members in the GCS sample, assigned using radial velocities, better than the background model.

The background model predicts the distribution of the observed parallax in Equation (8). For the foreground model, specified by an age, a metallicity, and optionally a value of the background contamination level, the predicted distribution is given by Equation (13), where the first factor is given by Equation (15) and the membership probabilities p_{ij} are calculated using the radial velocities.

In Figure 14, we show figures similar in spirit to Figure 7. For a few specially selected stars (high-probability members of the Sirius moving group) we have calculated the background prediction for the parallax (left panel in each row), the foreground prediction when fixing α at the value determined from the global contamination analysis (middle panel in each row), and the foreground prediction when fitting the background contamination (right panel in each row); in making these figures, we chose the best-fit parameters for the Sirius moving group from Table 1. The two stars in this figure are chosen to illustrate the model selection and do not reflect the general trend. The first row shows an example where the foreground model performs well: the foreground model with fixed α makes a good prediction for the parallax of this star and, by virtue of being narrow and informative, gives a higher probability to the observed parallax than the background model—note the difference in scale on the y-axes. The second row shows the much more common situation in which the foreground model misses completely and the observed parallax is found in the tails of the predicted distribution; the background model performs better by virtue of being broader.

We repeat this for all of the stars in the GCS sample. We only consider the 7577 stars with colors $B - V < 1$ mag. We marginalize over the parameters of the foreground model to compute the foreground probability of each parallax in the GCS sample and from this calculate the total probability of the parallaxes of stars in the GCS sample. The logarithm of this is given in Table 2 for each of the moving groups. Note that the prior distributions assumed for age, metallicity, and α do matter

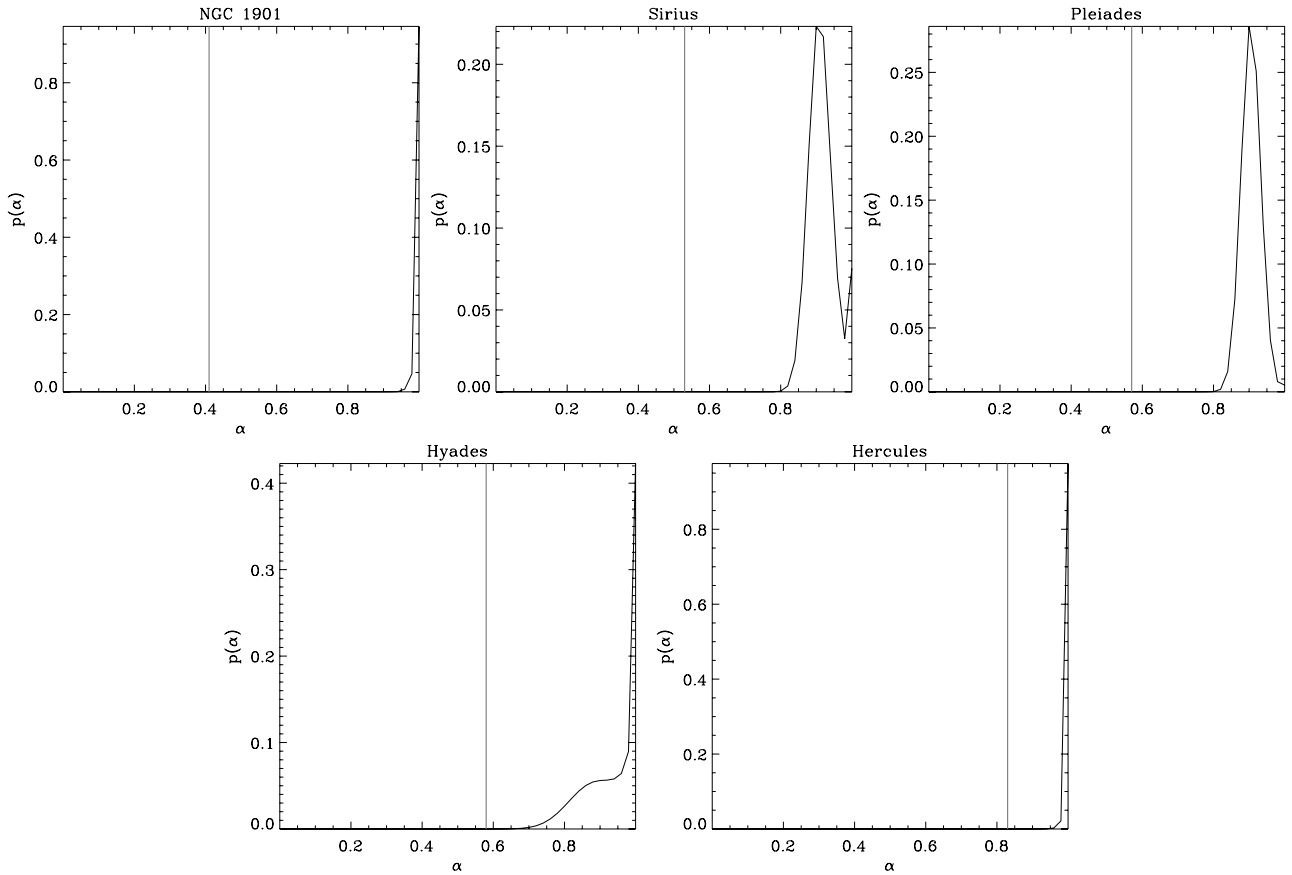

Figure 13. Posterior distribution for the background contamination level α for each of the moving groups, marginalized over age and metallicity of the foreground model with uniform priors on the metallicity and the logarithm of the age. Total contamination—$\alpha = 1$—is preferred in most cases. The value of α obtained from a global contamination analysis—the value used in Figure 11—is indicated by the vertical line.

now since these provide the integration measure on the space of properties through which we can integrate over these properties.

A first thing to note is that the foreground model when fixing α, both using only the best-fit values for the parameters as when marginalizing over the posterior distribution for the parameters of the foreground model, predicts the GCS parallaxes worse than the background model, except in the case of the Hercules moving group. That the Hercules moving group could be considered a single-burst stellar population is somewhat surprising, as it is generally regarded as the best established example of a moving group with a dynamical origin. The preference for the foreground model is only slight and the fact that, if left free, the background contamination parameter runs to $\alpha = 1$ is strong evidence against it being an evaporating cluster. When we let α be a free parameter, all of the foreground models perform at least as well as the background model, although only slightly for most groups. There might be a subsample of stars in each of the moving groups that is the remnant of a cluster of stars. However, at the best-fit background contamination levels in Table 1, hardly any stars are assigned to the moving groups when using the relevant hard cut on membership probability.

In the case of Hyades, even though the foreground model only performs as well as the background hypothesis, the best-fit foreground model is very similar to the Hyades cluster's properties, such that a subset of stars in the Hyades moving group may have originated from the open cluster. This is not entirely unexpected, as there must be *some* stars that have already been lost to the open cluster but that still share its space motion. However, this fraction is not simply equal to the difference between the best-fit values of α in Table 1 and one. In the analysis above, we did not remove open-cluster members from our sample, and, for example, 28 of the stars in our sample are confirmed Hyades members—they are part of the sample from Perryman et al. (1998) described in Section 3. These 28 stars make up 11% of the expected 261 Hyades members for this sample—they are all high-probability members of the Hyades moving group—comparable to the 14% of non-background found in the best fit to the Hyades moving group. These 28 stars were selected using a stringent membership criterion and therefore we can expect the actual number of Hyades-open-cluster members present in our sample to be even higher. Thus, we find that only a very insignificant fraction—at most a few percent—of a moving group can be explained by the evaporation of a single open cluster, in disagreement with the 15%–40%, for low- and intermediate-mass stars respectively, found by Famaey et al. (2007).

7. A RESONANT DYNAMICAL ORIGIN OF THE LOW-VELOCITY MOVING GROUPS

Now that we have firmly established that none of the moving groups can be entirely interpreted as being an evaporating open cluster, we can turn to investigating the possible dynamical origins of the moving groups. If not an evaporating moving cluster, the next most likely a priori explanation of the moving groups is that they are generated by one of the non-axisymmetric perturbations to the Galactic potential, e.g., by the bar or spiral arms. This is not to say that there are no other possible

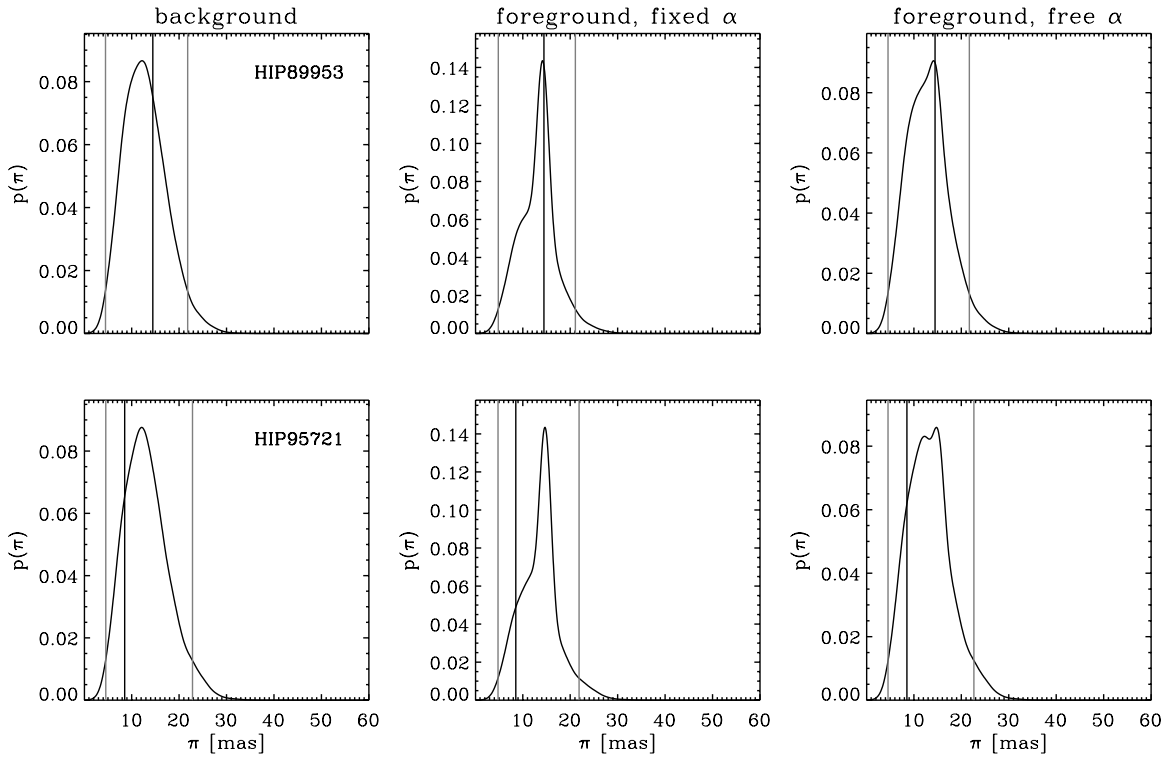

Figure 14. Model selection using the GCS sample: the background model prediction for two individual stellar parallaxes in the GCS sample is contrasted with the best-fit foreground single-burst stellar population model for a fixed value of the background contamination α and the best-fit value for α for the Sirius moving group (see Table 1 for the details of these best-fit single-burst stellar populations). The foreground models are trained using probabilistic moving-group assignments from the *Hipparcos* tangential velocities, while the GCS radial velocity is used to probabilistically assign the two GCS stars featured in this figure to moving groups. The top row shows an example where the informative foreground prediction does better than the broad background model prediction; the bottom row shows an example where the narrow foreground prediction is wrong and the uninformative background predictions performs better. In each panel, the probability of the parallax π is conditional on the star's positional, kinematic, and photometric data (except for the observed trigonometric parallax).

explanations of the moving groups' existence—e.g., projection effects of partially mixed phase-space structure (Tremaine 1999)—but theoretical work has suggested that moving groups naturally arise in various non-axisymmetric scenarios. As mentioned in Section 1, the evidence for the dynamical origin of the moving groups has been largely circumstantial, amounting to little more than finding that the moving groups display some variety of ages and metallicities. The purpose of this section is to test the hypothesis of a dynamical origin in a more specific, albeit generic, manner.

We can broadly distinguish between two classes of dynamical origin for the moving groups: those in which the moving groups are generated through steady-state non-axisymmetric perturbations and those in which they are due to transient perturbations. This section will mostly test the former category. Steady-state perturbations such as those associated with the bar or spiral structure are characterized by a pattern speed, which could potentially vary although this is not the case in any of the dynamical scenarios considered in the literature so far. Since orbits have associated natural frequencies—the radial and azimuthal frequencies in the plane, or the epicycle and angular frequencies in the epicycle approximation—strong interactions between the non-axisymmetric perturbations and the stars occur when these two sets of frequencies are commensurate, that is, when the difference between the perturbation's frequency and the angular or azimuthal frequency of the orbit is commensurate with the radial frequency. This gives rise to the co-rotation resonance, where the period of the perturbation is equal to the angular period of the orbit, and the Lindblad resonances, which are associated with closed orbits in the rotating frame

Table 2
Model Selection Using the GCS Sample: Is the Single-stellar-population Model for the Moving Groups Preferred?

Group	Best-fit SSP, fixed α	Marginalized SSP, fixed α	Best-fit SSP, free α	Marginalized SSP, free α
NGC 1901	−262	−262	17	17
Sirius	−61	−61	0	1
Pleiades	−70	−70	1	5
Hyades	−8	−8	0	0
Hercules	2	2	0	15

Notes. The difference between the logarithm of the probability of the parallaxes of the 7577 stars in the GCS sample used in Section 6 ($B - V < 1$ mag) under the various foreground models and that under the background model is given for each moving group. The logarithm of the likelihood of the background model is −23,155. "Marginalized" probabilities have the uncertainties in the best-fit values integrated out by marginalizing over the posterior distribution for age, metallicity, and, if applicable, background contamination level α.

of the perturbation that do not cross themselves (e.g., Binney & Tremaine 2008). The influence of a weak non-axisymmetric perturbation to the overall potential is therefore most strongly felt at these resonances (e.g., Lynden-Bell & Kalnajs 1972). If the moving groups' origin lies in steady non-axisymmetric perturbations, we would expect the Sun's present location to be near one of the resonances of the non-axisymmetric structure to account for its strong influence on the velocity distribution.

Simulations confirm this basic picture. Several simulations have shown that moving-group-like structures form near the resonances associated with the bar (e.g., Dehnen 2000; Fux

Table 3
High/Low Metallicity Model Selection: Do the Moving Groups have Higher or Lower Metallicities than the Background Disk Population?

Group	$R_c(L)$[a] (kpc)	Expected Δ[Fe/H][b] (dex)	Expected σ[Fe/H][b] (dex)	$\langle\Delta$[Fe/H]$\rangle$[c] (dex)	σ[Fe/H][c] (dex)	High Metallicity	Low Metallicity
NGC 1901	8.0	0.02	0.025	0.02	0.16	−203	−144
Sirius	8.5	−0.03	0.015	−0.03	0.15	−108	−8
Pleiades	7.6	0.05	0.015	0.02	0.16	−43	−37
Hyades	7.6	0.05	0.003	0.11	0.14	3	−14
Hercules	7.2	0.10	0.040	0.01	0.17	−40	−106

Notes. The difference between the logarithm of the probability of the parallaxes of the 9330 stars in the GCS sample (0.35 mag $< B - V <$ 0.95 mag) under the higher/lower metallicity foreground models and that under the background model is given for each moving group. The logarithm of the likelihood of the background model is −27,882.

[a] Galactocentric radius of the circular orbit with the same angular momentum as the center of the moving group.

[b] Expected metallicity anomaly and spread based on the mean radius ($\approx R_c(L)$), the velocity width of the moving group and a metallicity gradient of −0.1 dex kpc^{-1}.

[c] Average metallicity and spread of each moving group, computed by weighting the metallicities in the GCS sample with the membership probabilities (see Equation (18)). The width includes the measurement uncertainty, which is about 0.08 dex.

2001) or spiral structure (Quillen & Minchev 2005) or at the overlap of resonances of these two (Quillen 2003). Even though spiral arms are observed to start near the end of the bar in many galaxies, the pattern speeds of these two features are probably not strongly related in a dynamical sense, i.e., their resonances would generically be independent of each other because their pattern speeds are in general very different (Sellwood & Sparke 1988). Note that in order to explain the Hercules moving group as being due to the outer Lindblad resonance (OLR) of the bar and the lower velocity moving groups as being due to resonances of the spiral structure, the Sun would have to be in a rather special location in the Galaxy to be at exactly the right spot with respect to all of these. More observational evidence for either of these scenarios is thus needed to check that the velocity distribution is not being overfit.

It is instructive to see what happens to the orbits of stars that are near one of the resonances to understand what properties we expect the moving-group members to have if they are associated with a resonance of dynamical origin. Generically, in the neighborhood of a resonance we expect to see a bifurcation of the orbits into two families (Contopoulos 1975; Weinberg 1994; Kalnajs 1991). This bifurcation could be such that one of the families is on nearly circular orbits and the other significantly lagging with respect to the local standard of rest, as is the case near the OLR of the bar (Dehnen 2000), or it could be such that there are no longer any stars on nearly circular orbits and one family lags with respect to the local standard of rest, while the other family moves faster than purely circular location (in both cases, this is at the present location of the Sun in the successful dynamical scenarios). At azimuths where these two families cross, we expect to see streams in pairs in the velocity distribution.

Under the hypothesis of an OLR origin for the Hercules moving group, there is a family of orbits that are anti-aligned with the bar and spend most of their time inside the OLR, and there is a family of orbits that are aligned with the bar and spend most of its time outside the OLR (Contopoulos & Grosbøl 1989). When invoking steady-state spiral arms to explain the existence of the Hyades/Pleiades moving groups and the Coma Berenices (which we do not study in this paper because it did not show up at high significance in the reconstruction of the velocity distribution in BHR) or Sirius moving group, the Sun's present location is near the 4:1 ILR and there is one family of orbits that is elongated, square-shaped, and that spends most of the orbit outside of the ILR, and another family of orbits that is also elongated, square-shaped, and is more typically found inside the ILR (Contopoulos & Grosbøl 1986). Varying the parameters of the spiral structure, moving-group-like structure also forms for other types of orbits, but generically one family of orbits' mean radius is inside the resonance and the other family's mean radius is outside the resonance. This is even somewhat the case when the moving groups are created by the transient behavior of the bar—e.g., recent bar growth (Minchev et al. 2009)—although the situation is a lot messier in these cases because of the time-dependent nature of the problem.

Thus, if the moving groups are particular manifestations of the dynamics near the resonances of the bar or spiral structure, then the previous argument shows that the orbits of stars in the moving groups concern different and mostly non-overlapping regions of the Galaxy: stars that are part of moving groups that on average lag the local circular motion are near their apogalacticon, so their orbits will be mostly confined to the inner Galaxy. Stars in moving groups that are ahead of circular motion on average are near their perigalacticon, so these stars spend most of their orbits in the outer Galaxy. Therefore, we can expect the stellar populations of moving groups to be different depending on their position in the v_x–v_y plane, as these populations of stars are born in different physical conditions. We will test this hypothesis in this section.

Specifically, the hypothesis we set out to test is the following. If moving groups are associated with a family of orbits that either spend most of the orbits inside of the solar circle or outside of it, then, since stars reflect the conditions of the regions in which they are born, stars in moving groups will either have a higher than average metallicity, or lower than average metallicity because there is a metallicity gradient in the Galaxy, declining outward from the Galactic center (e.g., Shaver et al. 1983; Afflerbach et al. 1997; Nordström et al. 2004; Rudolph et al. 2006). For each moving group we can estimate this expected metallicity difference by calculating the mean metallicity at the mean radius of each moving group if it was moving in a simple axisymmetric potential. We can approximate this mean radius by the radius of the circular orbit that has the same angular momentum as the center of each moving group. The mean radii found by assuming a flat rotation curve with a circular velocity of 235 km s^{-1} and a distance to the Galactic center of 8.2 kpc (Bovy et al. 2009) are listed in Table 3. Assuming a metallicity gradient in [Fe/H] of −0.1 dex kpc^{-1} (e.g., Mayor

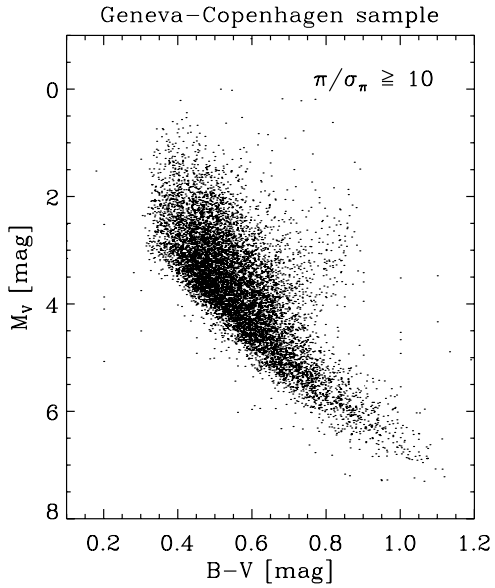

Figure 15. Color–magnitude diagram of the magnitude-limited GCS sample of 9575 stars used in Sections 7 and 8 with relative parallax uncertainties $\lesssim$10%.

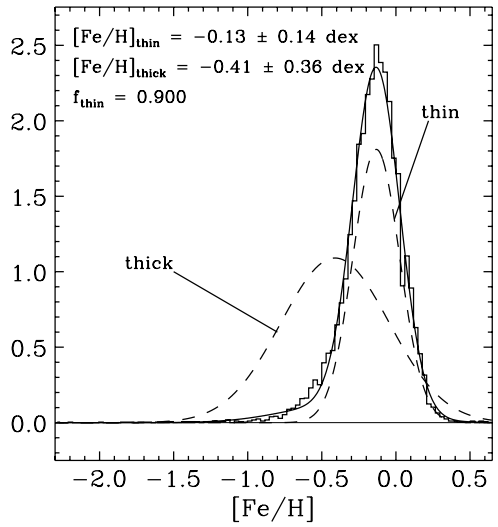

Figure 16. Metallicity distribution in the solar neighborhood: the distribution of metallicities of the 9575 stars in the GCS sample. The best-fit two-Gaussian decomposition is overlaid: the two components as the dashed lines (the "thin" disk component has been scaled down for clarity) and the resulting distribution as the full line. The parameters for the best-fit two-Gaussian distribution are given in the top-left corner as the mean ± standard deviation of each component.

1976; Nordström et al. 2004) these mean radii translate in the expected metallicity differences of a few hundreds of a dex to a tenth of a dex for Hercules in Table 3. In reality, we can expect these differences to be larger, since the resonance-trapped orbits will make larger excursions inward or outward than in this simple axisymmetric argument.

There will be some spread around this mean value, but this spread will certainly be smaller than the width of the full thin-disk metallicity distribution, which is, as we will show below, about 0.14 dex. We can estimate the expected width of a moving group's metallicity distribution based on its velocity width by using the same procedure that we used in the last paragraph. Using the velocity widths from BHR we find expected widths of a few hundreds of a dex or less; these are given in Table 3. These expected widths are smaller than the expected metallicity offset for each moving group except for NGC 1901. Therefore, we expect each moving groups' metallicity distribution to be largely contained in either the higher than average or lower than average part of the local thin disk metallicity distribution and this effect should be detectable.

Thus, we ask for each of the moving groups whether it is better fit by a model with a higher or lower metallicity than the background model, which reflects the full metallicity distribution in the solar neighborhood. Since the *Hipparcos* sample that we have been using throughout this paper does not include spectroscopic metallicity information, we use a sample selected from the GCS catalog instead. We use less conservative cuts on the binary and giant contamination of this sample to maximize the number of stars in the sample. Giant contamination is in fact very small in this sample of F and G dwarfs, and the presence of binaries is not really an issue since the multiple radial velocity epochs available for all stars in the GCS data allow for an accurate determination of the mean motion, although the photometric parallax technique that we use will be slightly biased by the presence of unresolved binaries. This affects both background and foreground models—foreground models in this section are those with low/high metallicities—and is taken care of in the non-parametric photometric parallax relation that we will again establish (all models effectively use a noise-in, noise-out approach as far as unresolved binaries are concerned).

As before we will train a non-parametric model to represent the background hypothesis—a non-parametric photometric parallax relation that we will establish for the GCS stars in exactly the same way that we trained the background model in Section 5. We cannot re-use the previous background model, as the GCS data are a much finer sampling in a narrow color range of the rich color–magnitude diagram than our previous *Hipparcos* sample. Rather than using a parametric model for the foreground hypothesis, we will build a non-parametric model similar to the background model by training it on stars that have higher or lower metallicity than average.

We construct the GCS sample used in this section as follows. From the GCS catalog we take all of the stars that have a *Hipparcos* counterpart and take their radial velocities with uncertainties and their metallicities from the GCS catalog (the latest reduction; Holmberg et al. 2007, 2009). We take the rest of the spatial, kinematic, and photometric data from the *Hipparcos* catalog (ESA 1997; van Leeuwen 2007). From this sample we select those stars with accurate parallaxes ($\pi/\sigma_\pi \geqslant 10$); this leaves a sample of 9575 stars. The color–magnitude diagram of these stars is shown in Figure 15.

The metallicity distribution of this sample is shown in Figure 16. Instead of taking a straight average of the metallicities, we fit it as a mixture of two components, anticipating a sizeable contribution from thick disk stars, which could skew the inferred average thin-disk metallicity. We perform this fit using the same deconvolution algorithm that we used to deconvolve the velocity distribution (Bovy et al. 2009b), assuming an uncertainty of 0.08 dex on the GCS [Fe/H] values. The resulting components are shown as the dashed curves in Figure 16, with arbitrary normalizations for display purposes. The best-fit parameters—mean and width of the two component Gaussians—are given in the top-left corner of the figure and the amplitude of the largest component is given as well. We can identify these two components with the thin and thick disks. The average thin disk metallicity is −0.13 dex with a spread of 0.14 dex. Note that because of the large amount of data, this mean thin disk metallicity can be considered to be very

well determined: an estimate of the uncertainty in the mean is $\sigma/\sqrt{f_{\rm thin}\,N}$, where $\sigma = 0.16$ dex is the width of the thin disk distribution convolved with the typical uncertainty in the GCS [Fe/H] values, $N = 9575$, and $f_{\rm thin} = 0.9$; the uncertainty in the mean is therefore about 0.002 dex. Of course, this uncertainty does not include the uncertainty in the thin–thick disk decomposition, but this is expected to be small.

To get a first sense of the metallicities of the various moving groups, we have computed the average metallicity of the stars in the GCS sample described in the previous section (before the color cut, but the results are the same after the color cut) by weighting the individual metallicities by the probability that the star is part of the moving group in question, i.e.,

$$\langle[\mathrm{Fe/H}]\rangle_j = \frac{\sum_i p_{ij}[\mathrm{Fe/H}]_i}{\sum_i p_{ij}}. \quad (18)$$

In the same way, we can calculate the second moment of the metallicity distribution of each moving group. These average metallicities and widths are given in Table 3. All of the moving groups except for Sirius have higher metallicities than the average thin disk metallicity, which we established above to be −0.13 dex. The Hyades moving group has a distinctively higher metallicity than average (see also Famaey et al. 2007, who find about the same value from a simple cut in velocity space); for the other moving groups, the difference is smaller and it is not clear what the significance of this result is. The fact that the second moment of each moving group's metallicity distribution is comparable to that of the full local metallicity distribution indicates that the moving groups' metallicity distributions are all very similar to that of the background. To test the significance of the non-zero offsets from the average metallicity, we perform a simple hypothesis test to see whether the moving groups' metallicities are significantly different from that of the general thin disk population.

We create two subsamples from the full sample of 9575 stars by taking the stars with metallicities larger than the average thin disk metallicity, and the stars with metallicities lower than the average; these samples contain 4593 and 4737 stars, respectively. That the latter suffers from some contamination from thick disk stars does not matter for our purposes as we are merely interested in creating a model with lower metallicities than the average thin disk.

We now fit a non-parametric photometric parallax relation to each of these samples—the background model consisting of all of the stars and the two foreground models consisting only of the low/high metallicity subsamples of the full sample—in exactly the same way as in Section 5. In order to avoid an excessively spiky non-parametric model, we focus on the color region $0.35\ \mathrm{mag} < B - V < 0.95$ mag in the color–magnitude diagram (see Figure 15). This cut only removes a very small number of stars (245 out of 9575), but makes sure that the optimal smoothing scale is not unduly affected by the sparse sampling of certain color regions. The width parameter of the Tricube kernel is again set by leave-one-out cross-validation.

As before, we can now calculate the total probability of the moving-group stars' parallaxes under the assumption that they are merely background stars, or under the assumption that they have higher than average or lower than average metallicities. The probability of an observed, trigonometric parallax based on the star's color, apparent magnitude and the full GCS training sample is again given by the expression in Equation (8), where the sum is now over the stars in the GCS sample (with the color cut discussed above). The probability of the observed parallax under the foreground model is again a mix between that of assuming the star has a higher/lower probability by virtue of being part of the moving group, and that of the background model, since we can only probabilistically assign membership. Thus, for each star the foreground probability is given by

$$p(\pi_{\mathrm{obs},i}|\mathrm{foreground}) = p(\pi_{\mathrm{obs},i}|\mathrm{high/low}\,Z)^{p_{ij}} \times p(\pi_{\mathrm{obs},i}|\mathrm{background})^{1-p_{ij}}, \quad (19)$$

where we now make use of the full kinematical information for the GCS stars, since we have all three components of the velocity to assign moving-group membership for this sample. The logarithm of the total probability under both foreground models and the background model thus calculated is tabulated in Table 3. If a moving group shows clear signs of a higher or lower metallicity, and thus of a resonant origin in a steady-state non-axisymmetric potential, we would expect the moving group's properties to be better fit by the higher/lower metallicity subsample than by the background model. As is clear from Table 3, no moving group shows convincing evidence that this is the case.

The only moving group that shows weak evidence that it has a different metallicity than the background of solar-neighborhood stars is the Hyades moving group, confirming the result for the Hyades found above by calculating a weighted average of the metallicities of Hyades members. That the Hyades moving group has a slight preference for a higher metallicity could indicate that it is associated with a family of orbits whose mean radii are within the solar circle, although the evidence is very weak. This may seem like a large factor, but one needs to consider that this is for a sample $\alpha_{\rm Hyades} N = 0.017 \times 9330 \approx 159$ stars. Nevertheless, since the two competing models are qualitatively similar, we conclude that there is some weak evidence here that the Hyades is made up of stars with higher than average metallicity.

The moving group which has the lowest likelihood of having either higher or lower metallicity than average is the NGC 1901 moving group. This is hardly surprising. The NGC 1901 moving group sits right on top of the bulk of the thin disk velocity distribution and it is therefore very hard to identify its members; its weight in the mixture of Gaussian decomposition of the velocity distribution is also rather large for a moving group, such that it was suggested in BHR that a large part of this Gaussian component might simply be part of the background distribution. The analysis here confirms this intuition.

As for the other moving groups, they are all best-fit by the background model, but we can nevertheless ask which of the two foreground models is preferred (ignoring the background model). The Sirius moving group prefers the low-metallicity foreground model over the high-metallicity model, confirming what we found above. Taken together with the result that the Hyades moving group has higher than average metallicity, this could be interpreted as tentative evidence in favor of the scenario in which these two moving groups arise through spiral perturbations near the ILR (as discussed above; Quillen & Minchev 2005). The evidence in favor of this explanation is not strong, but given the difficulty with which group membership is established through kinematic association, it may be compelling.

As for the Pleiades moving group, it has often been assumed that its origin is strongly linked to that of the Hyades moving group, since some reconstructions of the velocity distribution did not resolve the difference between the moving groups (Famaey et al. 2005) and because they are part of the same branch in

the Galactic-plane part of the velocity distribution (Skuljan et al. 1999). Although in the metallicity test performed here the Pleiades moving group is best fit by the background model, the runner-up is the foreground model with lower metallicity than average, as opposed to the best-fitting model for the Hyades, which has higher than average metallicity—note that this result is not confirmed by the calculation of the average metallicities above. This argues against a common origin for the Pleiades and Hyades moving groups. Recent bar growth has recently been proposed as a scenario in which the Hyades and Pleiades have a different origin (Minchev et al. 2009). Because of the transient nature of the effect of bar growth on the local velocity distribution, it is quite possible that the stars that make up the Pleiades moving group do not have a preference for a single metallicity at the present epoch.

Finally, we observe that the Hercules moving group, long thought to be a signature of the OLR of the bar and the moving group with the largest and most significant expected metallicity anomaly, is not preferentially fit by a model with higher metallicity than average, as would be the case if the resonant origin were correct, but is instead better fit by the background model. The background model is preferred by quite a large margin. Focusing only on the preferred foreground model, however, we see that the higher metallicity model is strongly preferred over the lower metallicity model. If one prefers to think that the overall preference for the background model is due to the difficulty of assigning group membership, or perhaps due to the slight offset between the Gaussian component identified in the reconstruction of the velocity distribution used here and other reconstructions of the velocity distribution, then this strong preference for the higher metallicity model over the lower metallicity model could be taken as evidence for the resonant origin of the Hercules moving group.

Because of the many assumptions and simplifications made in estimating the expected metallicity distribution of the various moving groups, the test we performed in this section is largely qualitative. Nevertheless, the fact that most of the moving groups are best fit by the background model as opposed to the higher or lower metallicity models challenges the explanation that the moving groups are associated with resonances related to the bar and/or spiral structure. If the moving groups nevertheless have a dynamical origin, then the dynamical effect is probably transient and less cleanly described in terms of supporting orbits. The predictions of the transient spiral or bar models in which moving groups arise in the literature (e.g., De Simone et al. 2004; Minchev et al. 2009) do not contain very definite descriptions of the expected stellar content of the moving groups generated through transient perturbations. Therefore, at this time it is hard to say whether these models are preferred by the data, but they do gain in likelihood if only because of the relative drop in likelihood of the resonant models due to their not being strongly supported by the data here.

8. HINTS OF RECURRENT SPIRAL STRUCTURE

If the solar neighborhood is currently near the ILR of the current cycle in the recurrent spiral structure scenario of Sellwood & Kahn (1991) described in Section 1, we would expect to see a feature in the local energy–angular-momentum distribution corresponding to stars being scattered at the ILR. Some tentative signs of this have been detected in the distribution of the *Hipparcos* stars (Sellwood 2000), although this analysis made use of the reconstruction of the local velocity distribution derived from tangential velocities alone by Dehnen (1998). With the full kinematical information in the GCS catalog, we can construct the energy–angular-momentum distribution without making any symmetry assumptions, and we can ask whether any of the moving groups are actually a manifestation of the groove feature in the angular-momentum distribution that drives spiral structure.

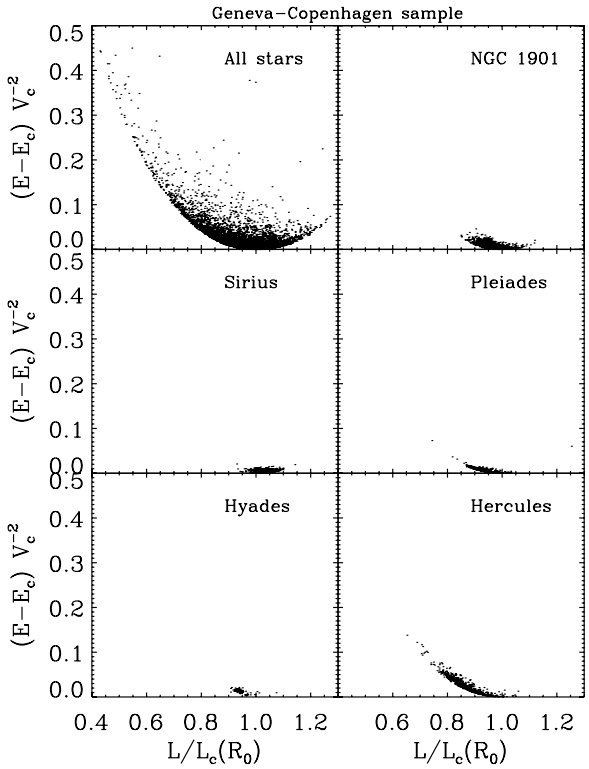

Figure 17. Lindblad diagram: distribution of the GCS stars in energy–angular-momentum space assuming a Mestel disk model for the Galaxy with circular velocity of 235 km s^{-1} and $R_0 = 8.2$ kpc; $E_c \equiv E_c(L)$ is the energy of a circular orbit with angular momentum L, $L_c(R_0)$ is the angular momentum of the circular orbit going through the Sun's present location. The location of high probability ($p_{ij} > 0.5$) members of the moving groups in this diagram is shown in the remaining panels. None of the moving groups stand out as a feature in this diagram.

In order to calculate the integrals of the motion of the stars in the GCS sample we need to assume a Galactic disk potential to convert positions and velocities into energy and angular momentum. We use a simple model for the disk potential, a Mestel disk (Mestel 1963; Binney & Tremaine 2008), which has a flat rotation curve and is uniquely characterized by the circular velocity; we assume a circular velocity at the Sun of $V_c = 235$ km s^{-1} and calculate Galactocentric distances using $R_0 = 8.2$ kpc (e.g., Bovy et al. 2009). The resulting distribution in energy and angular momentum of the 9575 GCS stars that was used in the previous section is shown in Figure 17. The lower cutoff in energy as a function of angular momentum is a selection effect: since the stars are all within about 100 pc from the Sun, stars on nearly circular orbits with angular momenta different from that at the solar circle do not make large enough excursions to make it into our sample.

We have also indicated the locations of the moving groups in this diagram, by making hard assignments of stars to moving groups using $p_{ij} > 0.5$, where p_{ij} is again calculated using the full three-dimensional velocity vector and the level of the hard cut is set to the value that gives an overall fraction of stars in moving groups of about 40%. There does not seem to be a clear scattering feature in this distribution. The Hercules

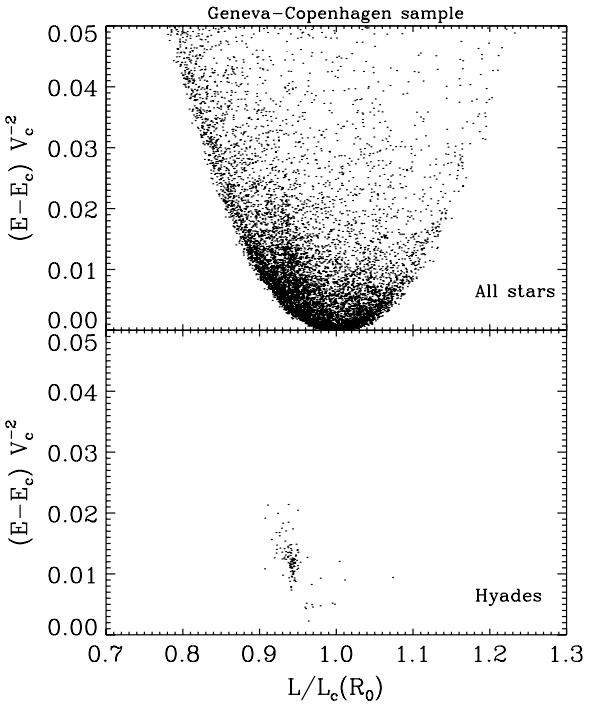

Figure 18. Close-up of Figure 17 for all stars and for the Hyades moving group. The Hyades members occupy a narrow range in angular momentum that corresponds to a feature in the distribution for all stars in the top panel.

moving group is, unsurprisingly, the only moving group that could potentially be associated with a scattering feature, but since it lies very close to the selection cutoff, it is hard to tell whether the Hercules moving group corresponds to a genuine scattering feature in this diagram or whether this is just the selection cutoff.

Recently, Sellwood (2010) has argued that the Hyades moving group rather than the Hercules moving group corresponds to the inner-Lindblad scattering feature. This feature is not apparent in Figure 17, since it concerns stars with an order of magnitude less random energy. For ease of comparison with Sellwood (2010), Figure 18 shows the GCS stars from Figure 17 with the smallest random motions, as well as the Hyades moving-group members. It is clear from this figure that the Hyades members do indeed correspond to the weak feature apparent in the top panel, confirming that the Hyades moving group might be a telltale sign of the recurrent nature of the Milky Way's spiral structure. This explanation does leave a few questions unanswered. The other low-velocity moving groups do not stand out in the energy–angular-momentum space. Ignoring the Hercules moving group, which can potentially be explained by the bar, how are the other moving groups formed if they are not the result of inhomogeneous star formation? Since the recurrent spiral structure is supposed to move inward, with the next spiral pattern's corotation radius near the inner Lindblad radius of the previous pattern, it is unlikely that the other moving groups are the result of scattering features associated with previous patterns since these features should be at larger values of the angular momentum and random energy. The result that the Hyades moving group is created by the scattering of stars at the ILR is also slightly at odds with the higher metallicity preference for the Hyades moving group found in Section 7: since stars are scattered inward at the ILR, the Hyades stars originate at greater Galactocentric radii and should therefore be, if anything, less metal-rich than average.

9. DISCUSSION AND FUTURE WORK

The tests and discussions above have all focused on determining the nature of the moving groups identified in Figure 1, and we have been able to rule out and provide support for some possible scenarios through which these moving groups may have formed. However, the groups shown in Figure 1 have been determined as Gaussian components in a deconvolution of the observed velocity distribution using 10 Gaussians. BHR found that the best-fitting mixture-of-Gaussians model contained only 10 components: when using more components, the velocity distribution was overfit as it became clear by testing its predictions of the external GCS radial-velocity data set. This does *not*, however, constitute an endorsement that the individual components have any physical interpretation: only the mixture itself, that is, the full distribution, can be considered real, the individual components are just positioned in such a way as to best describe the overall velocity distribution. It is therefore fair to ask whether the results in this paper have not been unduly influenced by our identification of moving groups with individual components of the mixture.

In BHR, we argued that moving groups can be associated with individual components of the mixture for a few different reasons. The overall reconstructed velocity distribution contains a number of distinct peaks (see Figure 1). These peaks can be unambiguously identified with specific components of the mixture, and therefore we can cross-correlate structures in the velocity distribution with the Gaussian components. Peaks, or overdensities, in the velocity distribution are what are generally called moving groups. Thus, since peaks in the velocity distribution are what define moving groups, and these peaks can be identified as individual components in the mixture, we can associate individual components with moving groups. Furthermore, the peaks in the velocity distribution compare favorably with the fiducial locations of the classical moving groups that are studied in this paper, although there are some small differences, such as that the Pleiades is resolved as two components, and that the Hercules moving group is both more smoothly connected to the bulk of the distribution than is generally thought to be the case and is located at slightly lower velocities than usual.

The generally accepted kinematic properties of the moving groups amount to not much more than a rough location and an even rougher estimate of the size and orientation of the moving group. The shape of the moving groups in the direction out of the plane is rarely discussed, although all of the moving groups' vertical velocities are presumably as well mixed as those of the general background population, because of the efficiency of phase mixing in the vertical direction. Similarly, until BHR, the weight of the individual moving groups in the velocity distribution, or even the total weight of the substructure in the distribution had never been quantitatively determined. It is hard to make quantitative estimates of group membership for individual stars, especially if not all of the velocity components of the stars are measured. The locations, shapes, and relative importance that we used in this paper allow for an objective way to estimate membership probabilities for a large sample of stars for all of the moving groups. While one can argue over whether these locations, shapes, and relative weights are exactly right for the moving groups, the objective, probabilistic procedure that we followed in this paper should be preferred over ad hoc choices on which to base membership assignments.

We also do not expect small biases in the parameters of the moving groups to affect the conclusions of this paper very

much. If the moving groups are actually located at slightly different locations in velocity space, if their profiles deviate from Gaussians in the wings, or if their relative weights are slightly higher or slightly lower than that which was assumed here, the computed membership probabilities will be somewhat incorrect, but not by large factors. That is, high-probability members based on the parameters that we assumed for the moving groups will remain high-probability members even for slightly different parameters. If the moving groups had shown a clear preference for an explanation of their existence over the others in the previous sections, e.g., if they were much better fit by a single-burst stellar population than by the background distribution, this conclusion would have stood out at high significance even if we computed the membership probabilities slightly incorrectly. Thus, the main conclusion of this paper—that no moving group shows clear evidence of having originated through one of the scenarios discussed here—holds whatever one believes about our parameterization. The more tentative conclusions reached here, however, should be interpreted with care.

Another caveat has to do with the possibility of radial mixing playing an important role in the chemical evolution of the Galactic disk. Radial mixing (Sellwood & Binney 2002) is the process in which stars can migrate radially from their birthplaces over large distances while remaining on nearly circular orbits. Such mixing causes a wider range of birth radii to be present at any Galactocentric radius and can therefore weaken expected correlations between, for example, metallicity and Galactocentric radius or metallicity and age (e.g., Roškar et al. 2008). Radial mixing occurs naturally in galactic disks with a transient spiral structure—only stars scattered at corotation can be scattered without increasing their random motion, so a large range of frequencies needs to be present for radial mixing to occur throughout the disk—but recently it has been shown that the coupling between a steady-state bar and steady-state spiral arms can also lead to significant radial migration (Minchev & Famaey 2009). In this scenario, stars from a wide range of birth radii and metallicities can migrate radially and be trapped into the bar's and spiral structure's resonances, leading to a potentially significant dilution of the metallicity-offset effect we searched for in Section 7. More work is necessary to test whether the resonance-overlap radial mixing is consistent with observations of the solar neighborhood (cf. Schoënrich & Binney 2009) and whether the metallicity distributions of the moving groups created by the resonances are consistent with the results from Section 7.

The scenarios discussed and explicitly tested here do not constitute an exhaustive set of the possible origins of the moving groups. We have only tested some of the simplest explanations for the existence of moving groups, but these simple explanations do command a considerable amount of weight in the discussion on the origin of the moving groups. Our tests considered all of the main classes of explanations for the origin of the moving groups; however, within these classes we did not test whether the moving groups are related to transient non-axisymmetric perturbations to the Galactic potential, nor did our test of the evaporating-cluster scenario include the possibility that the moving groups are the remnants of *several* open clusters. All of these alternative explanations provide a priori reasonable explanations of the moving groups' existence and should therefore be tested. Testing these explanations will be harder because the stellar content of the moving groups will have to be determined in greater detail than what has been done here. Theoretical work and simulations will also have to establish the nature of the moving groups in the scenarios where they are due to transient perturbations to allow the data on the stellar content of the moving groups to be interpreted in terms of these models.

Future work to elucidate the origin of the moving groups could go beyond the simple tests performed here by fitting more complicated models for the chemical composition and star formation history of each moving group. This "chemical tagging" (Freeman & Bland-Hawthorn 2002) could lead to greater insight into the kind of stars or orbits that make up the moving groups. Fitting these more general models will be considerably more complicated than what has been done here. Nevertheless, the probabilistic approach followed here in which all stars in the sample are carried through the analysis of each moving group with appropriate membership-probability weights—a weak cut could be done for computational efficiency—will be essential in these more sophisticated analyses to study the kinematic structures that are the moving groups.

10. CONCLUSIONS

We summarize our results as follows.

1. We use large samples of stars extracted from the *Hipparcos* and GCS catalogs to study the properties of the five most prominent low-velocity moving groups: the NGC 1901 group, the Sirius group, the Pleiades group, the Hyades group, and the Hercules group. Using membership probabilities calculated in a probabilistic manner based on the tangential velocities of the stars, the radial velocities, or both, and by propagating these membership probabilities through our whole analysis, we are able to use the maximum number of stars in the study of each moving group—an order of magnitude improvement for most of the moving groups—and avoid any possible biases that could result from making hard cuts on membership probabilities in analyses of this kind.
2. For the four moving groups in our sample with an associated open cluster, we asked whether the moving groups could consist of stars that have evaporated from these open clusters. By comparing the parallaxes of the stars that we predict, if the stars in the moving groups have the same age and metallicity as the open cluster that the moving group is associated with, with the observed trigonometric parallax, we establish that a large part of each moving group is poorly fit by the assumption that it has the same stellar population as the open cluster. This establishes beyond any reasonable doubt that the moving groups are *not* fundamentally associated with their eponymous open clusters.
3. Next, we studied whether each moving group could conceivably be associated with *any* open cluster, not necessarily the one normally associated with it. We constructed a background model in which the moving group is nothing more than a sparse sampling of the local disk population of stars and single-burst stellar population foreground models parameterized by an age, a metallicity, and a level of background contamination. For reasonable values of the background contamination, we find that only the Hercules moving group displays marginal evidence that it could be a remnant of a past star formation event. However, letting the level of background contamination run free, all of the moving groups prefer very large values of the contamination, reaching values close to complete contamination by the

background, especially in the case of the Hercules moving group. Therefore, we can confidently conclude that none of the moving groups is a remnant of a single open cluster.

4. To test scenarios in which moving groups are formed as a consequence of resonances associated with the bar and/or spiral structure, we asked whether the moving groups are better fit by a model with higher than average—or lower than average—metallicity, such as would generically be the case in resonant models for the moving groups. We find that of all the moving groups only the Hyades moving group shows a metallicity preference, and that is toward higher metallicity. All of the other moving groups are best represented by the background population of stars, although the Sirius moving group prefers a lower than average metallicity over higher than average, which together with the higher than average metallicity of the Hyades could be an indication of a spiral-structure-associated resonance origin for the Hyades and Sirius moving groups. The Pleiades moving group is preferably fit by a lower than average metallicity rather than a higher than average metallicity, arguing against a common origin for the Hyades and Pleiades moving groups. The Hercules moving group has a preference toward higher metallicity, consistent with it being associated with the OLR of the bar. We stress that all of this evidence is very tentative and the background model is the preferred model in most cases, raising the likelihood of transient non-axisymmetric perturbation scenarios for the origin of the moving groups.
5. We confirm the result of Sellwood (2010) that the Hyades moving groups might be associated with features—grooves—in the angular momentum distribution as would be expected in some models of recurrent spiral structure.

It is a pleasure to thank the anonymous referee for valuable comments and Michael Aumer, Mike Blanton, Iain Murray, and Sam Roweis for helpful discussions and assistance. Financial support for this project was provided by the National Aeronautics and Space Administration (grant NNX08AJ48G) and the National Science Foundation (grant AST-0908357). D.W.H. is a research fellow of the Alexander von Humboldt Foundation.

REFERENCES

Aarseth, S. J., & Woolf, N. J. 1972, Astrophys. Lett., 12, 159
Adams, J. D., Stauffer, J. R., Monet, D. G., Skrutskie, M. F., & Beichman, C. A. 2001, AJ, 121, 2053
Afflerbach, A., Churchwell, E., & Werner, W. M. 1997, ApJ, 478, 190
Allison, R. J., Goodwin, S. P., Parker, R. J., de Grijs, R., Portegies Zwart, S. F., & Kouwenhoven, M. B. N. 2009, ApJ, 700, L99
Antoja, T., Valenzuela, O., Pichardo, B., Moreno, E., Figueras, F., & Fernández, D. 2009, ApJ, 700, L78
Ascenso, J., Alves, J., & Lago, M. T. V. T. 2009, A&A, 495, 147
Asiain, R., Figueras, F., & Torra, J. 1999, A&A, 350, 434
Aumer, M., & Binney, J. J. 2009, MNRAS, 397, 1286
Bensby, T., Oey, M. S., Feltzing, S., & Gustafsson, B. 2007, ApJ, 655, L89
Bertelli, G., Bressan, A., Chiosi, C., Fagotto, F., & Nasi, E. 1994, A&AS, 106, 275
Binney, J., & Tremaine, S. 2008, Galactic Dynamics (2nd ed.; Princeton, NJ: Princeton Univ. Press)
Blaauw, A. 1970, in IAU Symp. 38, The Spiral Structure of our Galaxy, ed. W. Becker & I. Kontopoulos (Dordrecht: Reidel), 199
Boesgaard, A. M., & Budge, K. G. 1988, ApJ, 332, 410
Boesgaard, A. M., & Friel, E. D. 1990, ApJ, 351, 467
Bok, B. J. 1934, Harvard Circ., 384, 1
Bok, B. J. 1936, Observatory, 59, 76
Bok, B. J. 1946, MNRAS, 106, 61
Bonnell, I. A., & Davies, M. B. 1998, MNRAS, 295, 691
Bouvier, J., Stauffer, J. R., Martin, E. L., Barrado y Navascues, D., Wallace, B., & Bejar, V. J. S. 1998, A&A, 336, 490
Bouvier, J., et al. 2008, A&A, 481, 661
Bovy, J., Hogg, D. W., & Rix, H.-W. 2009, ApJ, 704, 1704
Bovy, J., Hogg, D. W., & Roweis, S. T. 2009a, ApJ, 700, 1794 (BHR)
Bovy, J., Hogg, D. W., & Roweis, S. T. 2009b, arXiv:0905.2979v1
Breger, M. 1968, PASP, 80, 578
Caloi, V., Cardini, D., D'Antona, F., Badiali, M., Emanuele, A., & Mazzitelli, I. 1999, A&A, 351, 925
Carlberg, R. G., & Sellwood, J. A. 1985, ApJ, 292, 79
Carraro, G., de La Fuente Marcos, R., Villanova, S., Moni Bidin, C., de La Fuente Marcos, C., Baumgardt, H., & Solivella, G. 2007, A&A, 466, 931
Chakrabarty, D. 2007, A&A, 467, 145
Chereul, E., & Grenon, M. 2001, in ASP Conf. Ser. 228, Dynamics of Star Clusters and the Milky Way, ed. S. Deiters, B. Fuchs, A. Just, R. Spurzem, & R. Wielen (San Francisco, CA: ASP), 398
Contopoulos, G. 1975, ApJ, 201, 566
Contopoulos, G., & Grosbøl, P. 1986, A&A, 155, 11
Contopoulos, G., & Grosbøl, P. 1989, A&AR, 1, 261
Dehnen, W. 1998, AJ, 115, 2384
Dehnen, W. 2000, AJ, 119, 800
Dehnen, W., & Binney, J. J. 1998, MNRAS, 298, 387
de la Fuente Marcos, R. 1995, A&A, 301, 407
De Silva, G. M., Freeman, K. C., Bland-Hawthorn, J., Asplund, M., & Bessell, M. S. 2007, AJ, 133, 694
De Simone, R., Wu, X., & Tremaine, S. 2004, MNRAS, 350, 627
de Zeeuw, P. T., Hoogerwerf, R., de Bruijne, J. H. J., Brown, A. G. A., & Blaauw, A. 1999, AJ, 117, 354
Dobbie, P. D., Kenyon, F., Jameson, R. F., Hodgkin, S. T., Hambly, N. C., & Hawkins, M. R. S. 2002, MNRAS, 329, 543
Eddington, A. S. 1910, MNRAS, 71, 43
Eggen, O. J. 1958, MNRAS, 118, 65
Eggen, O. J. 1993, AJ, 106, 1885
Eggen, O. J. 1996, AJ, 112, 1595
Elmegreen, D. M., & Elmegreen, B. G. 1983, MNRAS, 201, 1021
Elmegreen, D. M., & Elmegreen, B. G. 1983, ApJ, 267, 31
ESA 1997, The *Hipparcos* and *Tycho* Catalogues (ESA SP-1200; Noordwijk: ESA)
Famaey, B., Jorissen, A., Luri, X., Mayor, M., Udry, S., Dejonghe, H., & Turon, C. 2005, A&A, 430, 165
Famaey, B., Pont, F., Luri, X., Udry, S., Mayor, M., & Jorissen, A. 2007, A&A, 461, 957
Famaey, B., Siebert, A., & Jorissen, A. 2008, A&A, 483, 453
Feltzing, S., & Holmberg, J. 2000, A&A, 357, 153
Freeman, K., & Bland-Hawthorn, J. 2002, ARA&A, 40, 487
Fux, R. 2001, A&A, 373, 511
Gratton, R. 2000, in ASP Conf. Ser. 198, Stellar Clusters and Associations: Convection, Rotation, and Dynamos, ed. R. Pallavicini, G. Micela, & S. Sciortino (San Francisco, CA: ASP), 225
Hambly, N. C., Hodgkin, S. T., Cossburn, M. R., & Jameson, R. F. 1999, MNRAS, 303, 835
Hillenbrand, L. A., & Hartmann, L. W. 1998, ApJ, 492, 540
Høg, E., et al. 2000a, A&A, 355, L27
Høg, E., et al. 2000b, A&A, 357, 367
Hogg, D. W., Blanton, M. R., Roweis, S. T., & Johnston, K. V. 2005, ApJ, 629, 268
Holmberg, J., Nordström, B., & Andersen, J. 2007, A&A, 475, 519
Holmberg, J., Nordström, B., & Andersen, J. 2009, A&A, 501, 941
Jeans, J. H. 1915, MNRAS, 76, 70
Jeans, J. H. 1935, Observatory, 58, 108
Kalnajs, A. 1991, in Dynamics of Disc Galaxies, ed. B. Sundelius (Göteborg: Department of Astronomy and Astrophysics, Göteborg Univ.), 323
Kapteyn, J. C. 1905, British Assoc. Adv. Sci. Rep. A, 85, 257
King, J. R., Villarreal, A. R., Soderblom, D. R., Gulliver, A. F., & Adelman, S. J. 2003, AJ, 125, 1980
Lin, C. C., & Shu, F. H. 1964, ApJ, 140, 646
Lovelace, R. V. E., & Hohlfeld, R. G. 1978, ApJ, 221, 51
Lynden-Bell, D., & Kalnajs, A. J. 1972, MNRAS, 157, 1
Mädler, J. H. 1846, Astron. Nachr., 24, 213
Mädler, J. H. 1847, Untersuchungen über die Fixstern-systeme (Lepizig: Mitau)
Maíz Apellániz, J. 2006, AJ, 131, 1184
Marigo, P., Girardi, L., Bressan, A., Groenewegen, M. A. T., Silva, L., & Granato, G. L. 2008, A&A, 482, 883
Mayor, M. 1976, A&A, 48, 301
McMillan, S. L. W., Vesperini, E., & Portegies Zwart, S. F. 2007, ApJ, 655, L45
Meidt, S. E., Rand, R. J., & Merrifield, M. R. 2009, ApJ, 702, 277
Merrifield, M. R., Rand, R. J., & Meidt, S. E. 2006, MNRAS, 366, 17

Mestel, L. 1963, MNRAS, 126, 553
Minchev, I., Boily, C., Siebert, A., & Bienayme, O. 2009, MNRAS, submitted, arXiv:0909.3516v1
Minchev, I., & Famaey, B. 2009, ApJ, submitted, arXiv:0911.1794v1
Moeckel, N., & Bonnell, I. A. 2009, MNRAS, 396, 1864
Nordström, B., et al. 2004, A&A, 418, 989
Pavani, D. B., Bica, E., Dutra, C. M., Dottori, H., Santiago, B. X., Carranza, G., & Díaz, R. J. 2001, A&A, 374, 554
Percival, S. M., Salaris, M., & Groenewegen, M. A. T. 2005, A&A, 429, 887
Perryman, M. A. C., et al. 1998, A&A, 331, 81
Proctor, R. A. 1869, Proc. R. Soc., 18, 169
Quillen, A. C. 2003, AJ, 125, 785
Quillen, A. C., & Minchev, I. 2005, AJ, 130, 576
Raboud, D., Grenon, M., Martinet, L., Fux, R., & Udry, S. 1998, A&A, 335, L61
Rasmussen, C. E., & Williams, C. K. I. 2006, Gaussian Processes for Machine Learning (Cambridge, MA: MIT Press)
Reid, I. N., & Hawley, S. L. 1999, AJ, 117, 343
Reid, N. 1992, MNRAS, 257, 257
Roškar, R., Debattista, V. P., Quinn, T. R., Stinson, G. S., & Wadsley, J. 2008, ApJ, 684, L79
Rudolph, A. L., Fich, M., Bell, G. R., Norsen, T., Simpson, J. P., Haas, M. R., & Erickson, E. F. 2006, ApJS, 162, 346
Schoënrich, R., & Binney, J. J. 2009, MNRAS, 396, 203
Schwarzschild, K. 1907, Nachrichten von der Königlichen Gesellschaft der Wissenschaften zu Göttingen, 5, 614
Sellwood, J. A. 2000, Ap&SS, 272, 31
Sellwood, J. A. 2010, MNRAS, submitted, arXiv:1001.5197v1
Sellwood, J. A., & Binney, J. J. 2002, MNRAS, 336, 785
Sellwood, J. A., & Carlberg, R. G. 1984, ApJ, 282, 61
Sellwood, J. A., & Kahn, F. D. 1991, MNRAS, 250, 278
Sellwood, J. A., & Lin, D. N. C. 1989, MNRAS, 240, 991
Sellwood, J. A., & Sparke, L. S. 1988, MNRAS, 231, 25
Shaver, P. A., McGee, R. X., Newton, L. M., Danks, A. C., & Pottasch, S. R. 1983, MNRAS, 204, 53
Skuljan, J., Hearnshaw, J. B., & Cottrell, P. L. 1999, MNRAS, 308, 731
Soderblom, D. R., & Clements, S. D. 1987, AJ, 93, 920
Soderblom, D. R., & Mayor, M. 1993, AJ, 105, 226
Stone, M. 1974, J. R. Stat. Soc. B, 36, 111
Terlevich, E. 1987, MNRAS, 224, 193
Toomre, A. 1969, ApJ, 158, 899
Tremaine, S. 1999, MNRAS, 307, 877
van Leeuwen, F. 2007, Astrophysics and Space Science Library, Vol. 250, Hipparcos, the New Reduction of the Raw Data (Berlin: Springer)
Wielen, R. 1971, A&A, 13, 309
Wasserman, L. 2006, All of Nonparametric Statistics (New York: Springer)
Weinberg, M. D. 1994, ApJ, 420, 597
Williams, P. M. 1971, MNRAS, 153, 171